

The simplest of them all: $t\bar{t}W^\pm$ at NLO accuracy in QCD

Giuseppe Bevilacqua,^a Huan-Yu Bi,^b Heribertus Bayu Hartanto,^c Manfred Kraus^d and Malgorzata Worek^b

^a*MTA-DE Particle Physics Research Group, University of Debrecen, H-4010 Debrecen, PBox 105, Hungary*

^b*Institute for Theoretical Particle Physics and Cosmology, RWTH Aachen University, D-52056 Aachen, Germany*

^c*Institute for Particle Physics Phenomenology, Department of Physics, Durham University, Durham, DH1 3LE, UK*

^d*Physics Department, Florida State University, Tallahassee, FL 32306-4350, USA*

E-mail: giuseppe.bevilacqua@science.unideb.hu,

bihy@physik.rwth-aachen.de, heribertus.b.hartanto@durham.ac.uk,

mkraus@hep.fsu.edu, worek@physik.rwth-aachen.de

ABSTRACT: Recent measurements of the $pp \rightarrow t\bar{t}W^\pm$ process in multi-lepton final states, as performed by the ATLAS collaboration in the context of the Higgs boson studies in the $t\bar{t}H$ channel, have shown discrepancies between theoretical predictions and experimental data. Such discrepancies have been observed both in the overall normalisation as well as in the modelling of the $t\bar{t}W^\pm$ process. With the goal of understanding and resolving the modelling issues within the SM $t\bar{t}W^\pm$ process we report on the state-of-the-art NLO QCD computation for this process. Specifically, we calculate higher-order corrections to the $e^+\nu_e\mu^-\bar{\nu}_\mu e^+\nu_e b\bar{b}$ and $e^-\bar{\nu}_e\mu^+\nu_\mu e^-\bar{\nu}_e b\bar{b}$ final state at the LHC with $\sqrt{s} = 13$ TeV. In the computation off-shell top quarks are described by Breit-Wigner propagators, furthermore, double-, single- as well as non-resonant top-quark contributions along with all interference effects are consistently incorporated at the matrix element level. Results at NLO QCD accuracy are presented in the form of fiducial integrated and differential cross sections for two selected renormalisation and factorisation scale choices and three different PDF sets. The impact of the top quark off-shell effects on the $t\bar{t}W^\pm$ cross section is also examined by an explicit comparison to the narrow-width approximation.

KEYWORDS: NLO Computations, QCD Phenomenology, Heavy Quark Physics

Contents

1	Introduction	1
2	Outline of the calculations and cross-checks	4
3	LHC setup	7
4	Phenomenological results for $t\bar{t}W^+$	10
4.1	Fiducial cross sections	10
4.2	Differential distributions	16
4.3	PDF uncertainties	20
4.4	Off-shell versus on-shell top quark decay modelling	22
5	Phenomenological results for $t\bar{t}W^-$	25
6	Summary and Outlook	27

1 Introduction

Given the present values of collision energy and integrated luminosity at the Large Hadron Collider (LHC), the observation of the associated production of top quark pairs with a W^\pm boson becomes experimentally more and more accessible [1–4]. The immense amount of available phase space leads to production and identification of all top quark final states. Consequently, the LHC gives us finally the opportunity to scrutinise not only the strength but also the structure and the dynamics of $t\bar{t}W^\pm$ production. The $t\bar{t}W^\pm$ process allows for a direct measurement of the top quark coupling to W^\pm bosons as well as the study of the top quark charge asymmetry (A_c^t) [5]. At the leading order (LO) in perturbation theory the $t\bar{t}W^\pm$ production process can only occur via a $q\bar{q}'$ annihilation, thus, contributions from gluons in the initial states are not possible. The $gq/g\bar{q}'$ channels open up at next-to-leading order (NLO) in QCD but the gg production starts to be available only once the next-to-next-to-leading order (NNLO) in QCD contributions are incorporated. The absence of the symmetric gg channel in the leading terms of the perturbative expansion makes the resulting top quark charge asymmetry as evaluated at the NLO level significantly larger than in $t\bar{t}$ production. Thus, $t\bar{t}W^\pm$ can provide a powerful complementary way to measure A_c^t . The $t\bar{t}W^\pm$ process comprises multiple charged leptons, b -jets and missing transverse momentum due to neutrinos. As a result, besides A_c^t also the integrated charge asymmetry for the top decay products can be examined at the LHC, namely the b -jet asymmetry (A_c^b) and the charged lepton asymmetry (A_c^ℓ). Both asymmetries are very large and already present at the LO for this process. The polarisation and asymmetry effects in $t\bar{t}W^\pm$ production can additionally offer a useful handle to constrain new physics effects [5].

Furthermore, the $t\bar{t}W^\pm$ process constitutes an important background for the associated production of the Standard Model (SM) Higgs boson and the top quark pair [6–8]. Analyses of $t\bar{t}H$ and $t\bar{t}W^\pm$ production in multi-lepton final states, which have been recently performed by the ATLAS collaboration, have shown an overall higher normalisation for the $t\bar{t}W^\pm$ process [3] when compared with theoretical predictions provided by OPENLOOPS + SHERPA [9, 10] and/or MADGRAPH5_AMC@NLO [11]. The normalisation factors obtained for the $t\bar{t}W^\pm$ background by ATLAS for a very inclusive cut selection were 30%–70% higher than the theoretical predictions. Additional problems have been observed with the modelling of the final states in the phase space regions, that are dominated by $t\bar{t}W^\pm$ production [3]. Specifically, shape disagreements between the data and the $t\bar{t}W^\pm$ predictions from the Monte Carlo simulations have been observed for various distributions. The most important source of systematic uncertainties for the $t\bar{t}W^\pm$ process has been associated with the modelling of QCD radiation, b -jet multiplicity and W gauge boson charge asymmetry. The latter, for example, has been studied with the help of the total charge distribution. Taking into account the impact of the assumptions made on the $t\bar{t}W^\pm$ background modelling in the $t\bar{t}H$ cross section measurement an improved description of the former is essential to achieve higher precision in the future measurements.

Last but not least, the $t\bar{t}W^\pm$ process can lead to final states that contain two charged leptons (electrons or muons) of the same electric charge. Such signatures are referred to as same-sign leptons and are a relatively rare phenomenon in the SM. The SM processes that can be a source of such final states are $W^\pm Z$, ZZ , $W^\pm W^\pm jj$ as well as $t\bar{t}Z$ and $t\bar{t}W^\pm$ production. In the case of the $W^\pm W^\pm jj$ process two production modes are possible: QCD-induced production and production via vector-boson fusion. Finally, WWW , W^+W^-Z and ZZZ in various decay channels give rise to same-sign leptons with either additional leptons or jets. Even though SM processes leading to same-sign lepton final states have usually very small cross sections, they are indispensable in searches for physics beyond the SM (BSM). These BSM searches are often focused on the presence of two same-sign leptons, missing transverse momentum and two (light- or b -) jets [12–15]. The same-sign leptons signature is present in many new physics scenarios, among others, in R -conserving SUSY models and also in those with the explicit R -parity breaking [16–19]. Similar signatures are additionally predicted by non-SUSY models such as minimal Universal Extra Dimensions [20]. Same-sign leptons are also the signature for top-quark partners that are predicted in models where the Higgs is a pseudo-Goldstone boson [21]. They are essential for the production of the doubly charged Higgs bosons in the left-right symmetric model and in the Higgs triplet model [22]. Furthermore, same-sign leptons are unavoidable when searching for heavy Majorana neutrinos [23] and same-sign top quark pair resonances [24].

Given such rich phenomenological applications it is essential to describe all features of the $t\bar{t}W^\pm$ process as accurately as possible, in order to either deepen our understanding of the SM or maximise the sensitivity to deviations from it. To achieve this, theoretical calculations for the $t\bar{t}W^\pm$ process need to comprise all quantum effects already at the matrix element level. In addition, the size of higher-order corrections and theoretical uncertainties have to be carefully scrutinised in such a complex environment. Moreover, the choice of appropriate renormalisation and factorisation scales must be addressed to keep the process

under excellent theoretical control.

The goal of this paper is, therefore, to provide state-of-the-art NLO QCD predictions for the SM $t\bar{t}W^\pm$ process in the multi-lepton channel. More precisely, we shall calculate NLO QCD corrections to the $e^+\nu_e\mu^-\bar{\nu}_\mu e^+\nu_e b\bar{b}$ and $e^-\bar{\nu}_e\mu^+\nu_\mu e^-\bar{\nu}_e b\bar{b}$ final state. In the calculation, for the first time, all double-, single- and non-resonant Feynman diagrams will be consistently taken into account together with the off-shell effects of the top quarks. Additionally, non-resonant and off-shell effects related to the W gauge bosons will be incorporated. This calculation constitutes the first fully realistic NLO QCD computation for top quark pair production with the additional W^\pm gauge boson.

As a final comment, we note that NLO QCD corrections to the inclusive $t\bar{t}W^\pm$ process, with the on-shell top quarks, have been calculated for the first time in [25] and afterwards recomputed in [5, 6]. Theoretical predictions for $t\bar{t}W^\pm$ at NLO in QCD have been additionally matched with shower MC programs using either the POWHEG method or the MC@NLO framework [6, 26]. In all cases top quark and W gauge boson decays have been treated in the parton shower approximation omitting the NLO $t\bar{t}$ spin correlations. Finally, in Ref. [27] improved calculations for the process have been presented. Specifically, NLO QCD corrections to the production and decays of top quarks and W gauge bosons have been included with full spin correlations in the narrow-width approximation (NWA). Besides NLO QCD corrections, a further step towards a more precise modelling of the on-shell $t\bar{t}W^\pm$ production process has been achieved by including either NLO electroweak corrections [28] and the subleading electroweak corrections [29, 30] or by incorporating soft gluon resummation effects with the next-to-next-to-leading logarithmic (NNLL) accuracy [31–33]. Very recently subleading electroweak corrections together with the $t\bar{t}$ spin-correlation effects for the on-shell $t\bar{t}W^\pm$ production matched to parton shower programs have been examined in the multi-lepton channel [34]. Top quark and W gauge boson decays have been realised via parton showers within the MADSPIN framework [35], which allowed to account for the leading-order spin correlations.

The paper is organised as follows. In Section 2 we briefly outline the framework of the calculation and discuss cross-checks that have been performed. The theoretical setup for LO and NLO QCD results is given in Section 3. Phenomenological results for $t\bar{t}W^+$ are discussed in detail in Section 4. They are provided for the LHC centre of mass system energy of $\sqrt{s} = 13$ TeV and for two renormalisation and factorisation scale choices as well as for the following three parton distribution functions (PDFs): NNPDF3.0, MMHT14 and CT14. Theoretical uncertainties due to the scale dependence and PDFs are also discussed in Section 4 both for the integrated and differential fiducial $t\bar{t}W^+$ cross sections. Additionally, in Section 4 the impact of the off-shell effects on the $t\bar{t}W^+$ cross section is examined. Section 5 is devoted to results for $t\bar{t}W^-$ production. In this case only theoretical predictions for the integrated fiducial cross sections are presented so as not to extend the length of the manuscript unnecessarily. This is well justified by the fact that the NLO QCD effects for $t\bar{t}W^+$ and $t\bar{t}W^-$ are very similar. Finally, in Section 6 our results for the $t\bar{t}W^\pm$ production process are summarised and conclusions are outlined.

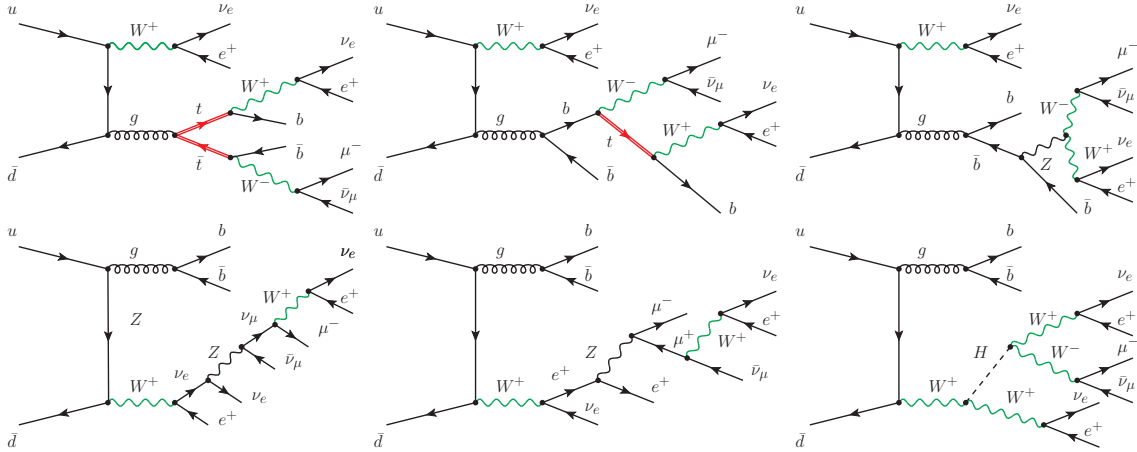


Figure 1. Representative tree level Feynman diagrams for the $pp \rightarrow e^+ \nu_e \mu^- \bar{\nu}_\mu e^+ \nu_e b \bar{b}$ process at $\mathcal{O}(\alpha_s^2 \alpha^6)$. In the first row diagrams with two (first diagram), only one (second diagram), or no (last diagram) top-quark resonances are presented. The double lines indicate the top and anti-top quark. In the second row diagrams that involve the W gauge boson resonance are given (first and the second diagram). They contribute to the finite W width corrections. The last diagram in the second row comprises the Higgs-exchange contribution that appears even though the b quarks are treated as massless partons.

2 Outline of the calculations and cross-checks

We compute the NLO QCD corrections to the full hadronic process $pp \rightarrow e^+ \nu_e \mu^- \bar{\nu}_\mu e^+ \nu_e b \bar{b}$. We consider the tree-level amplitude at $\mathcal{O}(\alpha_s^2 \alpha^6)$. The $e^+ \nu_e \mu^- \bar{\nu}_\mu e^+ \nu_e b \bar{b}$ final state¹ is produced via the scattering of one up-type quark and the corresponding down-type anti-quark. The quark-gluon initial state opens up only at the next order in α_s . Due to the large gluon luminosity this might have a potentially large impact on the size of the higher-order corrections and theoretical uncertainties. Unlike for the processes $pp \rightarrow t\bar{t}j/t\bar{t}\gamma/t\bar{t}Z/t\bar{t}H$, the production process $t\bar{t}W^+$ only originates from the gluon-gluon initial state starting from NNLO. At the LO, however, we distinguish 4 partonic subprocesses for the full hadronic process. All partonic subprocesses can be obtained from $q\bar{q}' \rightarrow e^+ \nu_e \mu^- \bar{\nu}_\mu e^+ \nu_e b \bar{b}$ by substituting different quark flavours ($q = u, d, c, s$). Each subprocess involves 556 tree Feynman diagrams. Examples of Feynman diagrams for the $u\bar{d} \rightarrow e^+ \nu_e \mu^- \bar{\nu}_\mu e^+ \nu_e b \bar{b}$ partonic subprocess are depicted in Figure 1. Even though we treat b quarks as massless partons there are Higgs-boson-exchange Feynman diagrams, see e.g. the last diagram in the second row of Figure 1. Once this contribution is also taken into account the number of diagrams increases to 564. To regularise intermediate top-quark resonances in a gauge-invariant way we employ the complex-mass scheme [36–39], which consistently describes off-shell top quark contributions by the Breit-Wigner distribution. All matrix elements are evaluated using

¹We shall concentrate here on the $t\bar{t}W^+$ process, however, a similar description applies to $t\bar{t}W^-$ production. We note here that the integrated fiducial cross section for $t\bar{t}W^+$ is larger than the one for $t\bar{t}W^-$. This can be easily understood by looking at the partonic subprocesses and the corresponding PDFs as well as their impact on the pp collisions at the LHC with $\sqrt{s} = 13$ TeV. We also note that at LO $t\bar{t}W^-$ is produced via $\bar{u}d$ and $\bar{c}s$.

One-loop correction type	Number of Feynman diagrams
Self-energy	7708
Vertex	4236
Box-type	2606
Pentagon-type	1116
Hexagon-type	260
Heptagon-type	16
Total number	15942

Table 1. *The number of one-loop Feynman diagrams for the $u\bar{d} \rightarrow e^+\nu_e\mu^-\bar{\nu}_\mu e^+\nu_e b\bar{b}$ partonic subprocess at $\mathcal{O}(\alpha_s^3\alpha^6)$ for the $pp \rightarrow e^+\nu_e\mu^-\bar{\nu}_\mu e^+\nu_e b\bar{b} + X$ process. The Higgs boson exchange contributions are not taken into account and the Cabibbo-Kobayashi-Maskawa mixing matrix is assumed to be diagonal.*

the complex top-quark mass μ_t defined by

$$\mu_t^2 = m_t^2 - im_t\Gamma_t. \quad (2.1)$$

The W and Z gauge bosons, on the other hand, are treated within the fixed width scheme, see e.g. [40]. Since we are interested in NLO QCD corrections the naive use of Breit-Wigner propagators for gauge bosons does not introduce problems in the calculations. The preservation of gauge symmetries (Ward Identities) by this approach has been explicitly checked up to the one-loop level. The calculation of the scattering amplitudes for the $q\bar{q}' \rightarrow e^+\nu_e\mu^-\bar{\nu}_\mu e^+\nu_e b\bar{b}$ process is based on the well-known off-shell Dyson-Schwinger iterative algorithm that is implemented within the HELAC-NLO framework [41] and in the HELAC-PHEGAS MC program [42]. The latter MC library is used to cross check all LO results. Phase space integration is performed and optimised with the help of PARNI [43] and KALEU [44].

The virtual corrections can be classified into self-energy, vertex, box-type, pentagon-type, hexagon-type and heptagon-type corrections. In Table 1 we provide the number of one-loop Feynman diagrams, that corresponds to each topology for the following partonic subprocess $u\bar{d} \rightarrow e^+\nu_e\mu^-\bar{\nu}_\mu e^+\nu_e b\bar{b}$. These numbers have been generated with the help of the QGRAF program [45], which generates Feynman diagrams for various types of QFT models. The 1-loop corrections have been evaluated by the HELAC-1LOOP [46] MC library, which incorporates CUTTOOLS [47, 48] and ONELOOP [49]. We have cross-checked our results with the publicly available general purpose MC program MADGRAPH5-AMC@NLO. Specifically, we have compared results for the virtual NLO contribution to the squared amplitude, $2\Re(\mathcal{M}_{\text{tree}}^*\mathcal{M}_{\text{one-loop}})$, for a few phase-space points for the $u\bar{d}$ partonic subprocess. For all phase-space points that we have tested perfect agreement has been found.

For the calculation of the real emission contributions, the package HELAC-DIPOLES [50] is employed. It comprises the dipole formalism of Catani and Seymour [51, 52] for arbitrary helicity eigenstates and colour configurations of the external partons and the Nagy-Soper subtraction scheme [53], which makes use of random polarisation and colour sampling of the external partons. Two independent subtraction schemes allow us to cross check the correctness of the real corrections by comparing the two results. Furthermore, a restriction on the phase space of the subtraction term is considered for both Catani-Seymour and Nagy-Soper schemes and additionally used for cross checks, see Ref. [54] and Ref. [55] for technical details of our implementation. The real correction process $pp \rightarrow e^+ \nu_e \mu^- \bar{\nu}_\mu e^+ \nu_e b \bar{b} j$ receives contributions from the following 12 partonic subprocesses

$$\begin{aligned}
gq &\rightarrow e^+ \nu_e \mu^- \bar{\nu}_\mu e^+ \nu_e b \bar{b} q', \\
g\bar{q}' &\rightarrow e^+ \nu_e \mu^- \bar{\nu}_\mu e^+ \nu_e b \bar{b} \bar{q}, \\
q\bar{q}' &\rightarrow e^+ \nu_e \mu^- \bar{\nu}_\mu e^+ \nu_e b \bar{b} g.
\end{aligned}
\tag{2.2}$$

Each subprocess comprises 3736 Feynman diagrams. As for the number of Catani-Seymour dipoles and Nagy-Soper subtraction terms we have respectively 12 and 4 for the first two subprocesses as well as 15 and 5 for the third one. The difference between the number of Catani-Seymour dipoles and Nagy-Soper subtraction terms corresponds to the total number of possible spectators that are only relevant in the Catani-Seymour subtraction scheme.

To summarise, our computational system is based on HELAC-1LOOP and HELAC-DIPOLES, which are both parts of the HELAC-NLO MC program. Let us note here, that among the processes of associated $t\bar{t}$ production which have been calculated so far with HELAC-NLO ($t\bar{t}X$, where $X = j, \gamma, Z, W^\pm$ [56–59]), $t\bar{t}W^\pm$ is perhaps the simplest one in terms of computational complexity. We draw this conclusion after comparing various criteria, such as the number of Feynman diagrams and subtraction terms involved in the calculation, or the number of partonic subprocesses and color structures of the amplitudes. Yet, computing NLO QCD corrections for the $t\bar{t}W^\pm$ process with the complete off-shell effects included, is challenging and requires a good computer cluster in order to accomplish the task in a reasonable amount of time. For this reason we store our theoretical predictions in the form of events, available in the format of either (modified) Les Houches Event Files [60] or ROOT Ntuples [61]. Expanding on methods presented in Ref. [62], each event is stored with additional matrix-element and PDF information which allows on-the-fly reweighting for different choices of scales and PDFs. In this way one can obtain predictions for arbitrary infrared-safe observables, kinematical cuts, renormalisation/factorisation scales and PDFs, without requiring additional rerunning of the computationally intense HELAC-NLO code. A user-friendly program, named HEPLLOT [63], has been developed to easily obtain physical predictions out of these event files. Both the event files and the HEPLLOT program are available upon request and might be directly used for experimental analyses at the LHC as well as to obtain accurate SM predictions in phenomenological studies on, e.g., Higgs boson or BSM physics.

3 LHC setup

We start with the $t\bar{t}W^+$ production process that is calculated at NLO in QCD for the LHC Run II energy of $\sqrt{s} = 13$ TeV. Specifically, the following final state is considered: $e^+\nu_e\mu^-\bar{\nu}_\mu e^+\nu_e b\bar{b} + X$ at perturbative order $\mathcal{O}(\alpha_s^3\alpha^6)$. By choosing different lepton generations for $W^+ \rightarrow e^+\nu_e$ and $W^- \rightarrow \mu^-\bar{\nu}_\mu$ we avoid virtual photon singularities stemming from the $\gamma \rightarrow e^+e^-$ and $\gamma \rightarrow \mu^+\mu^-$ decays. However, we have checked by an explicit LO calculation that these interference effects are at per-mil level. The complete cross section for the $pp \rightarrow \ell^+\nu_\ell \ell^-\bar{\nu}_\ell \ell^+\nu_\ell b\bar{b}$ process, where ℓ^\pm stands for $\ell^\pm = e^\pm, \mu^\pm$, can be obtained by multiplying the results from this paper with a lepton-flavour factor of 8. We do not take into account the τ leptons. The large variety of final states into which the tau leptons can decay makes them very challenging to reconstruct and identify at hadron colliders [64, 65]. For this reason they are often studied separately at the LHC. Additionally, we have examined the impact of the Higgs boson contributions on the $pp \rightarrow e^+\nu_e\mu^-\bar{\nu}_\mu e^+\nu_e b\bar{b}$ fiducial cross section. We have checked that, at LO with $m_H = 125$ GeV and $\Gamma_H = 4.07 \times 10^{-3}$ GeV, the latter contribute at the level of per-mille. Furthermore, for a variety of differential distributions, which we have examined, differences between theoretical results with and without these contributions were within the integration errors for our setup. Consequently, in the following we shall neglect the Higgs boson contribution both at the LO and NLO. For our calculation we keep the Cabibbo-Kobayashi-Maskawa (CKM) mixing matrix diagonal. We have checked, however, the impact of off-diagonal contributions on the fiducial cross sections using LO and NLO calculations in the NWA. We use the approximation for the CKM matrix that considers mixing only between the first two generations of quarks, with the Cabibbo angle $\sin\theta_C = 0.225686$. By employing HELAC-NLO and taking into consideration additional subprocesses we have established that off-diagonal contributions are at the 2% level at LO and below 1.5% at NLO. These findings have been cross-checked with the MCFM Monte Carlo program [66]. Following recommendations of the PDF4LHC Working Group for the usage of PDFs suitable for applications at the LHC Run II [67] we employ CT14 [68], MMHT14 [69] and NNPDF3.0 [70]. In particular, we use NNPDF30-nlo-as-0118 with $\alpha_s(m_Z) = 0.118$ (NNPDF30-1o-as-0130 with $\alpha_s(m_Z) = 0.130$) as the default PDF set at NLO (LO). In addition, we present results for CT14nlo and MMHT14nlo68clas118 at NLO as well as CT141lo and MMHT141o68c1 at LO. The running of the strong coupling constant α_s with two-loop (one-loop) accuracy at NLO (LO) is provided by the LHAPDF interface [71]. The number of active flavours is set to $N_F = 5$ and the following SM parameters are used

$$\begin{aligned}
 G_\mu &= 1.166378 \cdot 10^{-5} \text{ GeV}^{-2}, & m_t &= 172.5 \text{ GeV}, \\
 m_W &= 80.385 \text{ GeV}, & \Gamma_W^{\text{NLO}} &= 2.09767 \text{ GeV}, \\
 m_Z &= 91.1876 \text{ GeV}, & \Gamma_Z^{\text{NLO}} &= 2.50775 \text{ GeV}.
 \end{aligned}
 \tag{3.1}$$

For the W and Z gauge boson width, Γ_W^{NLO} and Γ_Z^{NLO} , we use the NLO QCD values as calculated respectively for $\mu_R = m_W$ and $\mu_R = m_Z$. We utilise them for LO and NLO matrix elements. All other partons, including bottom quarks, and leptons are treated as massless particles. The LO and NLO top quark widths for the off-shell case are calculated

according to formulae from Ref. [39, 72, 73] and are given by

$$\Gamma_{t,\text{off-shell}}^{\text{LO}} = 1.45759 \text{ GeV}, \quad \Gamma_{t,\text{off-shell}}^{\text{NLO}} = 1.33247 \text{ GeV}. \quad (3.2)$$

On the other hand, for the NWA case we use the following values

$$\Gamma_{t,\text{NWA}}^{\text{LO}} = 1.48063 \text{ GeV}, \quad \Gamma_{t,\text{NWA}}^{\text{NLO}} = 1.35355 \text{ GeV}. \quad (3.3)$$

The top quark width is treated as a fixed parameter throughout this work. Its value corresponds to a fixed scale $\mu_R = m_t$, that characterises the top quark decays, and is equal to $\alpha_s(m_t) = 0.107671$. The $\alpha_s(m_t)$ parameter is independent of $\alpha_s(\mu_0)$ that goes into the matrix element calculations as well as PDFs, since the latter describes the dynamics of the whole process. Let us add here as well that, while calculating the scale dependence for the NLO cross section, Γ_t^{NLO} is kept fixed independently of the scale choice. The error introduced by this treatment is, however, of higher order and particularly for two scales $\mu = m_t/2$ and $\mu = 2m_t$ is below 1.5% as we have checked by the explicit NLO calculation in the NWA. Consequently, omitting the variation of $\Gamma_{t,\text{NWA}}^{\text{NLO}}$ can underestimate the NLO scale dependence maximally by 1.5%. The electromagnetic coupling α is calculated from the Fermi constant G_μ , i.e. in the G_μ -scheme, via

$$\alpha_{G_\mu} = \frac{\sqrt{2}}{\pi} G_F m_W^2 \sin^2 \theta_W, \quad (3.4)$$

where $\sin^2 \theta$ is defined according to

$$\sin^2 \theta = 1 - \frac{m_W^2}{m_Z^2}, \quad (3.5)$$

and G_μ is extracted from the muon decay. Fixed-order calculations at NLO in QCD contain a residual dependence on the renormalisation (μ_R) and the factorisation scale (μ_F). This dependence arises from the truncation of the perturbative expansion in α_s . For that reason observables depend on the values of μ_R and μ_F . They have to be provided as input parameters, and can generally be functions of the external momenta. The uncertainty on higher orders is estimated by varying μ_R and μ_F independently around a central scale μ_0 in the range

$$\frac{1}{2} \leq \frac{\mu_R}{\mu_0}, \frac{\mu_F}{\mu_0} \leq 2. \quad (3.6)$$

It is conventional to require the following additional condition to be met

$$\frac{1}{2} \leq \frac{\mu_R}{\mu_F} \leq 2. \quad (3.7)$$

We search for the minimum and maximum of the resulting cross sections. Because none of the ratios μ_F/μ_0 , μ_R/μ_0 and μ_R/μ_F can be larger than two or smaller than one-half it is sufficient to consider the following pairs only

$$\left(\frac{\mu_R}{\mu_0}, \frac{\mu_F}{\mu_0} \right) = \left\{ (2, 1), (0.5, 1), (1, 2), (1, 1), (1, 0.5), (2, 2), (0.5, 0.5) \right\}. \quad (3.8)$$

For the central value of μ_0 we consider two cases. First, we employ a fixed scale given by

$$\mu_0 = m_t + \frac{m_W}{2}. \quad (3.9)$$

The scale choice $\mu_0 = m_t + m_V/2$, where V stands for a massive boson ($V = H, Z, W^\pm$), has previously been used in higher order calculations for $pp \rightarrow t\bar{t}V$ production with on-shell top quarks [27, 74–79]. Thus, we follow this prescription as well. Our second choice for the scale is dynamical, i.e. phase-space dependent. The scale is chosen to be the scalar sum of all transverse momenta in the event, including the missing transverse momentum. We denote this scale as H_T . Not only the functional form of μ_0 is important but also the overall factor that stands in front. To this end, we select

$$\mu_0 = \frac{H_T}{3}, \quad (3.10)$$

where H_T is given by

$$H_T = p_T(\ell_1) + p_T(\ell_2) + p_T(\mu^-) + p_T^{miss} + p_T(j_{b_1}) + p_T(j_{b_2}), \quad (3.11)$$

where ℓ labels positrons. The choice we make is blind to the fact that in the $pp \rightarrow e^+\nu_e\mu^-\bar{\nu}_\mu e^+\nu_e b\bar{b}$ process top-quark resonances might appear. Thus, it seems to be a more natural option for the process with the complete top-quark off-shell effects included. It should play a vital role especially in the case of various dimensionful observables in the high p_T phase space regions where the single- and non-resonant contributions comprise a significant part of the integrated cross section. At times they can even be larger than the double-resonant contribution. We note that H_T from Eq. (3.11) is directly measurable, i.e. it is defined with the help of observable final states that pass all the cuts that we shall specify in the following. Furthermore, since the electron and the muon reconstruction and charge identification can be performed at the LHC with very high efficiency [81, 82], we can distinguish between μ^- and e^+ in our studies. To differentiate between the two positrons, however, the ordering in p_T is introduced. The same applies to the two b -jets that are present in the final state. Consequently, in Eq. (3.11) j_{b_1} and j_{b_2} stand for the hardest and the softest b -jet, μ^- labels the muon, $\ell_{1,2}$ corresponds to the hardest and the softest positron and p_T^{miss} is the missing transverse momentum, which is built out of two ν_e 's and a $\bar{\nu}_\mu$. We define jets out of all final-state partons with pseudo-rapidity $|\eta| < 5$. In particular, partons are recombined into jets via the IR-safe *anti- k_T* jet algorithm [80] where the separation parameter $R = 0.4$ is used. We require exactly two b -jets and three charged leptons, two of which are same-sign charged leptons. All final states have to fulfil the following selection criteria that mimic the ATLAS detector response

$$\begin{aligned} p_T(\ell) &> 25 \text{ GeV}, & p_T(j_b) &> 25 \text{ GeV}, \\ |y(\ell)| &< 2.5, & |y(j_b)| &< 2.5, \\ \Delta R(\ell\ell) &> 0.4, & \Delta R(\ell j_b) &> 0.4, \end{aligned} \quad (3.12)$$

where ℓ stands for the charged lepton $\ell = \mu^-, e^+$. Such selection would ensure well observed isolated charged leptons and b -jets in the central rapidity regions of the ATLAS detector. We put no restriction on the kinematics of the extra (light) jet and the missing transverse momentum.

4 Phenomenological results for $t\bar{t}W^+$

4.1 Fiducial cross sections

We generate theoretical predictions for the LHC that is a pp collider, thus, the rates for $t\bar{t}W^+$ and $t\bar{t}W^-$ are not equal. We start with the $t\bar{t}W^+$ production process as it has the largest cross section between the two. We begin the presentation of our results with a discussion of the integrated fiducial cross section for the fixed scale choice. With the input parameters and cuts specified as in Section 3, we arrive at the following predictions if the NNPDF3.0 PDF sets are employed

$$\begin{aligned}\sigma_{e^+\nu_e\mu^-\bar{\nu}_\mu e^+\nu_e b\bar{b}}^{\text{LO}}(\text{NNPDF3.0}, \mu_0 = m_t + m_W/2) &= 106.9_{-20.5}^{+27.7} \begin{matrix} (26\%) \\ (19\%) \end{matrix} [\text{scale}] \text{ ab}, \\ \sigma_{e^+\nu_e\mu^-\bar{\nu}_\mu e^+\nu_e b\bar{b}}^{\text{NLO}}(\text{NNPDF3.0}, \mu_0 = m_t + m_W/2) &= 123.2_{-8.7}^{+6.3} \begin{matrix} (5\%) \\ (7\%) \end{matrix} [\text{scale}] \begin{matrix} +2.1 \\ -2.1 \end{matrix} \begin{matrix} (2\%) \\ (2\%) \end{matrix} [\text{PDF}] \text{ ab}.\end{aligned}\tag{4.1}$$

For the MMHT14 PDF sets we obtain instead

$$\begin{aligned}\sigma_{e^+\nu_e\mu^-\bar{\nu}_\mu e^+\nu_e b\bar{b}}^{\text{LO}}(\text{MMHT14}, \mu_0 = m_t + m_W/2) &= 102.2_{-19.9}^{+27.0} \begin{matrix} (26\%) \\ (19\%) \end{matrix} [\text{scale}] \text{ ab}, \\ \sigma_{e^+\nu_e\mu^-\bar{\nu}_\mu e^+\nu_e b\bar{b}}^{\text{NLO}}(\text{MMHT14}, \mu_0 = m_t + m_W/2) &= 123.1_{-8.4}^{+5.9} \begin{matrix} (5\%) \\ (7\%) \end{matrix} [\text{scale}] \begin{matrix} +2.8 \\ -2.5 \end{matrix} \begin{matrix} (2\%) \\ (2\%) \end{matrix} [\text{PDF}] \text{ ab}.\end{aligned}\tag{4.2}$$

Finally, with the CT14 PDF sets our results are as follows

$$\begin{aligned}\sigma_{e^+\nu_e\mu^-\bar{\nu}_\mu e^+\nu_e b\bar{b}}^{\text{LO}}(\text{CT14}, \mu_0 = m_t + m_W/2) &= 103.8_{-19.7}^{+26.7} \begin{matrix} (26\%) \\ (19\%) \end{matrix} [\text{scale}] \text{ ab}, \\ \sigma_{e^+\nu_e\mu^-\bar{\nu}_\mu e^+\nu_e b\bar{b}}^{\text{NLO}}(\text{CT14}, \mu_0 = m_t + m_W/2) &= 122.9_{-8.6}^{+6.0} \begin{matrix} (5\%) \\ (7\%) \end{matrix} [\text{scale}] \begin{matrix} +3.0 \\ -3.5 \end{matrix} \begin{matrix} (2\%) \\ (3\%) \end{matrix} [\text{PDF}] \text{ ab}.\end{aligned}\tag{4.3}$$

We do not provide the LO PDF uncertainties because they are similar to the NLO values, i.e. an order of magnitude smaller than the LO theoretical uncertainties due to scale dependence. For the NNPDF3.0 PDF sets we obtain positive and moderate NLO QCD corrections of the order of 15%. For the MMHT14 PDF set instead we receive 20% and for CT14 18% corrections. Scale uncertainties taken as the maximum of the lower and upper bounds are at the 26% level at the LO. After inclusion of the NLO QCD corrections, they are reduced down to 7%. Another source of theoretical uncertainties comes from the PDF parametrisation. Using the error PDF sets the NLO PDF uncertainties have been calculated separately for NNPDF3.0, MMHT14 and CT14. They are rather small at the level of 2%–3%. We should mention here, that the CT14 PDF uncertainties are provided as 90% confidence level intervals, therefore, we have rescaled them by a factor 1.645 to compare with other PDF sets, for which uncertainties are provided as 68% confidence level intervals. We can further notice, that NLO results for three different PDF sets are very consistent as the differences among them are at the per-mill level only. Overall, the PDF uncertainties for the process under consideration are well below the theoretical uncertainties due to the scale dependence, which remain the dominant source of the theoretical systematics.

$$\mu_R = \mu_F = \mu_0 = m_t + m_W/2$$

PDF	$p_T(j_b)$	σ^{LO} [ab]	δ_{scale}	σ^{NLO} [ab]	δ_{scale}	δ_{PDF}	$\sigma^{\text{NLO}}/\sigma^{\text{LO}}$
CT14	25	103.8	+26.7 (26%) -19.7 (19%)	122.9	+6.0 (5%) -8.6 (7%)	+3.0 (2%) -3.5 (3%)	1.18
	30	96.3	+24.8 (26%) -18.4 (19%)	112.8	+5.2 (5%) -7.6 (7%)	+2.8 (2%) -3.3 (3%)	1.17
	35	88.1	+22.7 (26%) -16.8 (19%)	102.3	+4.4 (4%) -6.8 (7%)	+2.5 (2%) -2.9 (3%)	1.16
	40	79.7	+20.7 (26%) -15.3 (19%)	91.8	+3.8 (4%) -6.0 (7%)	+2.3 (2%) -2.6 (3%)	1.15
MMHT14	25	102.2	+27.0 (26%) -19.9 (19%)	123.1	+5.9 (5%) -8.4 (7%)	+2.8 (2%) -2.5 (2%)	1.20
	30	94.8	+25.0 (26%) -18.5 (19%)	113.0	+5.0 (4%) -7.5 (7%)	+2.5 (2%) -2.3 (2%)	1.19
	35	86.8	+23.0 (27%) -16.9 (19%)	102.5	+4.3 (4%) -6.7 (7%)	+2.3 (2%) -2.0 (2%)	1.18
	40	78.5	+20.9 (27%) -15.3 (20%)	91.9	+3.7 (4%) -5.9 (6%)	+2.0 (2%) -1.8 (2%)	1.17
NNPDF3.0	25	106.9	+27.7 (26%) -20.5 (19%)	123.2	+6.3 (5%) -8.7 (7%)	+2.1 (2%) -2.1 (2%)	1.15
	30	99.2	+25.8 (26%) -19.1 (19%)	113.1	+5.4 (5%) -7.8 (7%)	+1.9 (2%) -1.9 (2%)	1.14
	35	90.8	+23.7 (26%) -17.5 (19%)	102.6	+4.7 (5%) -6.8 (7%)	+1.7 (2%) -1.7 (2%)	1.13
	40	82.1	+21.5 (26%) -15.9 (19%)	92.0	+4.0 (4%) -6.1 (7%)	+1.6 (2%) -1.6 (2%)	1.12

Table 2. LO and NLO integrated fiducial cross sections for the $pp \rightarrow e^+ \nu_e \mu^- \bar{\nu}_\mu e^+ \nu_e b\bar{b} + X$ process at the LHC with $\sqrt{s} = 13$ TeV. Results are evaluated using $\mu_R = \mu_F = \mu_0$ with $\mu_0 = m_t + m_W/2$. Three PDF sets and four different values of the $p_T(j_b)$ cut are used. Also given are theoretical uncertainties coming from the scale variation (δ_{scale}) and from PDFs (δ_{PDF}). In the last column the \mathcal{K} -factor, defined as $\sigma^{\text{NLO}}/\sigma^{\text{LO}}$, is shown.

In Table 2 a stability test of LO and NLO fiducial cross sections with respect to the b -jet transverse momentum cut is shown for $\mu_0 = m_t + m_W/2$ and for three PDF sets. The cut is varied in steps of 5 GeV within the following range $p_T(j_b) \in (25 - 40)$ GeV. We denote theoretical uncertainties as estimated from the scale variation by δ_{scale} and from PDFs by δ_{PDF} . Also given is the \mathcal{K} -factor, defined as $\mathcal{K} = \sigma^{\text{NLO}}/\sigma^{\text{LO}}$. Regardless of the PDF set employed we observe that NLO QCD corrections are almost constant in size.

$$\mu_R = \mu_F = \mu_0 = H_T/3$$

PDF	$p_T(j_b)$	σ^{LO} [ab]	δ_{scale}	σ^{NLO} [ab]	δ_{scale}	δ_{PDF}	$\sigma^{\text{NLO}}/\sigma^{\text{LO}}$
CT14	25	111.7	+29.3 (26%) -21.6 (19%)	124.1	+3.9 (3%) -7.5 (6%)	+3.0 (2%) -3.5 (3%)	1.11
	30	103.3	+27.1 (26%) -20.0 (19%)	113.5	+3.3 (3%) -6.6 (6%)	+2.8 (2%) -3.2 (3%)	1.10
	35	94.1	+24.7 (26%) -18.2 (19%)	102.7	+3.0 (3%) -5.9 (6%)	+2.5 (2%) -2.9 (3%)	1.09
	40	84.6	+22.3 (26%) -16.4 (19%)	91.9	+2.7 (3%) -5.2 (6%)	+2.2 (2%) -2.6 (3%)	1.09
MMHT14	25	110.0	+29.6 (27%) -21.7 (20%)	124.3	+3.9 (3%) -7.4 (6%)	+2.7 (2%) -2.4 (2%)	1.13
	30	101.8	+27.4 (27%) -20.1 (20%)	113.7	+3.3 (3%) -6.6 (6%)	+2.5 (2%) -2.2 (2%)	1.12
	35	92.8	+25.0 (27%) -18.3 (20%)	102.9	+3.0 (3%) -5.8 (6%)	+2.3 (2%) -2.0 (2%)	1.11
	40	83.4	+22.5 (27%) -16.5 (20%)	92.1	+2.7 (3%) -5.1 (6%)	+2.0 (2%) -1.8 (2%)	1.10
NNPDF3.0	25	115.1	+30.5 (26%) -22.5 (20%)	124.4	+4.3 (3%) -7.7 (6%)	+2.1 (2%) -2.1 (2%)	1.08
	30	106.5	+28.2 (26%) -20.8 (20%)	113.9	+3.5 (3%) -6.8 (6%)	+1.9 (2%) -1.9 (2%)	1.07
	35	97.0	+25.7 (27%) -18.9 (20%)	103.1	+3.1 (3%) -6.0 (6%)	+1.7 (2%) -1.7 (2%)	1.06
	40	87.2	+23.2 (27%) -17.0 (20%)	92.3	+2.8 (3%) -5.3 (6%)	+1.5 (2%) -1.5 (2%)	1.06

Table 3. *As in Table 2 but for $\mu_R = \mu_F = \mu_0 = H_T/3$.*

Moreover, higher-order theoretical predictions show a very stable behaviour with respect to theoretical uncertainties. In particular, no large differences can be observed between the results obtained for the highest value of the $p_T(j_b)$ cut and for the default value of 25 GeV. This suggests that the perturbative expansion for the process at hand is not spoiled by the appearance of large logarithms, thus, under excellent theoretical control. Having established the stability of the NLO QCD results with respect to the $p_T(j_b)$ cut for the fixed scale choice we move on to the dynamical scale choice, that we have adopted for our studies.

Using the same input parameters and cuts as before but employing $\mu_0 = H_T/3$ the

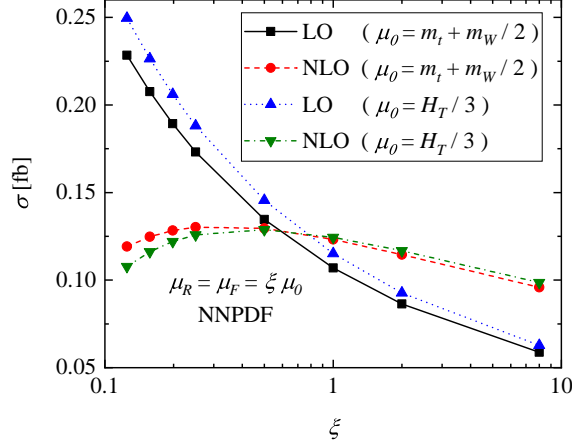


Figure 2. Scale dependence of the LO and NLO integrated fiducial cross section for the $pp \rightarrow e^+\nu_e\mu^-\bar{\nu}_\mu e^+\nu_e b\bar{b} + X$ production process at the LHC with $\sqrt{s} = 13$ TeV. Renormalisation and factorisation scales are set to the common value $\mu_R = \mu_F = \mu_0$ with $\mu_0 = m_t + m_W/2$ and $\mu_0 = H_T/3$. The LO and NLO NNPDF3.0 PDF sets are employed.

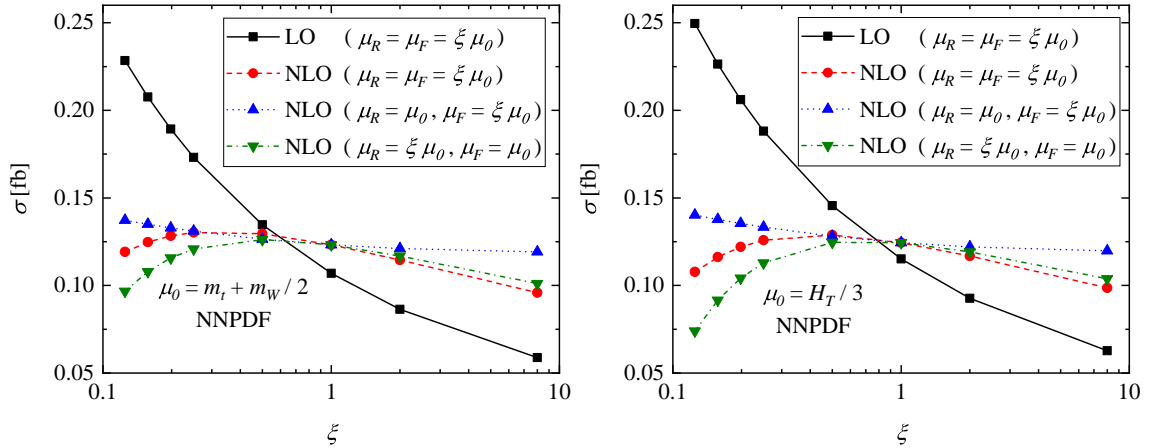


Figure 3. Scale dependence of the LO and NLO integrated fiducial cross section for the $pp \rightarrow e^+\nu_e\mu^-\bar{\nu}_\mu e^+\nu_e b\bar{b} + X$ production process at the LHC with $\sqrt{s} = 13$ TeV separately for $\mu_0 = m_t + m_W/2$ and $\mu_0 = H_T/3$. The LO and NLO NNPDF3.0 PDF sets are employed. For each case of μ_0 also shown is the variation of μ_R with fixed μ_F and the variation of μ_F with fixed μ_R .

results for the $pp \rightarrow e^+\nu_e\mu^-\bar{\nu}_\mu e^+\nu_e b\bar{b}$ process for the default NNPDF3.0 PDF sets can be summarised as follows

$$\begin{aligned}
\sigma_{e^+\nu_e\mu^-\bar{\nu}_\mu e^+\nu_e b\bar{b}}^{\text{LO}}(\text{NNPDF3.0}, \mu_0 = H_T/3) &= 115.1^{+30.5 (26\%)}_{-22.5 (20\%)} [\text{scale}] \text{ ab}, \\
\sigma_{e^+\nu_e\mu^-\bar{\nu}_\mu e^+\nu_e b\bar{b}}^{\text{NLO}}(\text{NNPDF3.0}, \mu_0 = H_T/3) &= 124.4^{+4.3 (3\%)}_{-7.7 (6\%)} [\text{scale}]^{+2.1 (2\%)}_{-2.1 (2\%)} [\text{PDF}] \text{ ab}.
\end{aligned}
\tag{4.4}$$

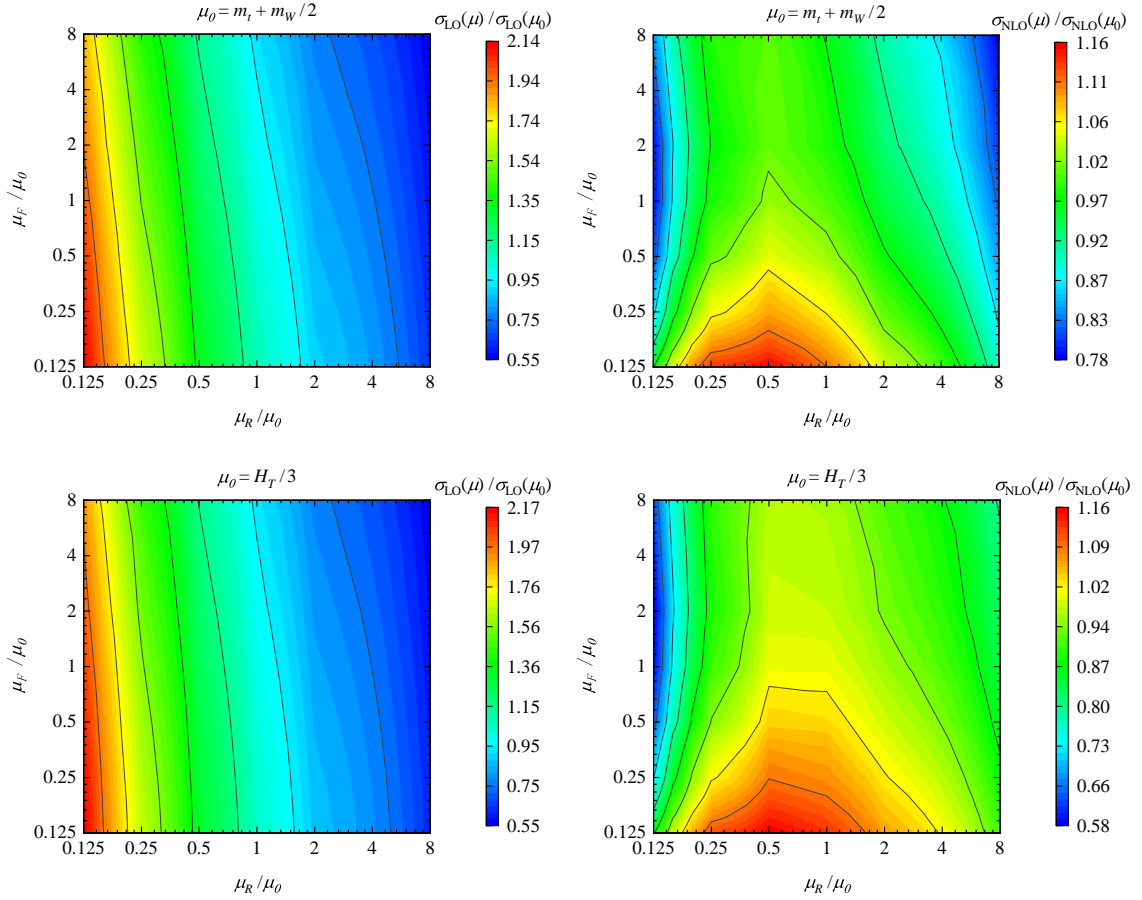


Figure 4. Integrated fiducial cross section for the $pp \rightarrow e^+\nu_e \mu^-\bar{\nu}_\mu e^+\nu_e b\bar{b} + X$ process at the LHC with $\sqrt{s} = 13$ TeV as a function of μ_R and μ_F . Results are evaluated using $\mu_0 = m_t + m_W/2$ and $\mu_0 = H_T/3$. The LO and NLO NNPDF3.0 PDF sets are employed.

For the MMHT14 PDF sets, on the other hand, we have

$$\begin{aligned} \sigma_{e^+\nu_e \mu^-\bar{\nu}_\mu e^+\nu_e b\bar{b}}^{\text{LO}}(\text{MMHT14}, \mu_0 = H_T/3) &= 110.0^{+29.6 (27\%)}_{-21.7 (20\%)} [\text{scale}] \text{ ab}, \\ \sigma_{e^+\nu_e \mu^-\bar{\nu}_\mu e^+\nu_e b\bar{b}}^{\text{NLO}}(\text{MMHT14}, \mu_0 = H_T/3) &= 124.3^{+3.9 (3\%)}_{-7.4 (6\%)} [\text{scale}]^{+2.7 (2\%)}_{-2.4 (2\%)} [\text{PDF}] \text{ ab}. \end{aligned} \quad (4.5)$$

Lastly, for the CT14 PDF sets we can report on the following predictions

$$\begin{aligned} \sigma_{e^+\nu_e \mu^-\bar{\nu}_\mu e^+\nu_e b\bar{b}}^{\text{LO}}(\text{CT14}, \mu_0 = H_T/3) &= 111.7^{+29.3 (26\%)}_{-21.6 (19\%)} [\text{scale}] \text{ ab}, \\ \sigma_{e^+\nu_e \mu^-\bar{\nu}_\mu e^+\nu_e b\bar{b}}^{\text{NLO}}(\text{CT14}, \mu_0 = H_T/3) &= 124.1^{+3.9 (3\%)}_{-7.5 (6\%)} [\text{scale}]^{+3.0 (2\%)}_{-3.5 (3\%)} [\text{PDF}] \text{ ab}. \end{aligned} \quad (4.6)$$

Results with $\mu_0 = H_T/3$ and for the NNPDF3.0 PDF set are a bit higher, as they increased by 8% at LO and by 1% at NLO when compared with results from Table 2. This is perfectly within the theoretical error estimates at the corresponding perturbative order. Moreover, the \mathcal{K} -factor obtained with this new scale is smaller, of the order of $\mathcal{K} = 1.08$. This is the

consequence of the larger shift in the normalisation of the LO cross section, which depends more strongly on the changes in μ_R and μ_F . The size of the NLO QCD corrections is rather stable and increases up to 11% – 13% for CT14 and MMHT14 respectively. As for the theoretical uncertainties from the scale dependence and from PDFs they are at the same level as for the fixed scale choice. Differences between predictions for various PDF sets are of the order of 3% – 5% at LO and 0.1% – 0.2% at NLO. Thus, internal PDF uncertainties as calculated separately for NNPDF3.0, MMHT14 and CT14 are an order of magnitude larger. Still, uncertainties due to scale dependence are the dominant source of theoretical systematics.

The integrated LO and NLO fiducial cross sections for the $pp \rightarrow e^+ \nu_e \mu^- \bar{\nu}_\mu e^+ \nu_e b \bar{b} + X$ production process for the dynamical scale choice are shown in Table 3 for four different values of the $p_T(j_b)$ cut. Also for $\mu_0 = H_T/3$ we observe a very stable behaviour of the cross section with respect to the higher-order corrections. Moreover, theoretical uncertainties do not show any sensitivity to changes in the $p_T(j_b)$ cut value.

In Figure 2 we present the result for the scale dependence graphically for $\mu_0 = m_t + m_W/2$ and $\mu_0 = H_T/3$. The behaviour of LO and NLO cross sections for the default NNPDF3.0 PDF sets is presented upon varying the μ_R and μ_F scales simultaneously by a factor ξ in the following range $\xi \in \{0.125, \dots, 8\}$. As already discussed, at LO the dependence is large illustrating the well known fact that the LO prediction can only provide a rough estimate. A significant reduction in the scale uncertainty is observed when NLO QCD corrections are included.

In Figure 3 we display again the dependence of the integrated LO and NLO fiducial cross sections on the variation of the fixed and dynamical scales for the NNPDF3.0 PDF set. This time, however, we show additionally NLO results with individual variation of μ_R and μ_F . Each time we plot two extra curves, the first one corresponds to the case where μ_R is kept fixed at the central value, while μ_F is varied and the second one describes the opposite situation. We can observe that regardless of the scale choice the scale variation is due to changes in both μ_R and μ_F . Thus, it is not driven solely by the renormalisation scale.

The dependence of the LO and NLO cross sections on μ_R and μ_F , which are varied this time independently but simultaneously around a central value of the scale, is presented in Figure 4. We plot distributions of the LO and NLO cross sections in the $\mu_R - \mu_F$ plane. On top of the previous three special cases i) $\mu_R = \mu_F = \xi\mu_0$, ii) $\mu_R = \mu_0$, $\mu_F = \xi\mu_0$ and iii) $\mu_F = \mu_0$, $\mu_R = \xi\mu_0$, here all cases in between are depicted as well. These contour plots provide complementary information to the previous scale dependence plots. We can see that at LO, independently of the scale choice, the fiducial cross section decreases only mildly with increasing μ_F , while it decreases rapidly with the increment of μ_R . Thus, the LO cross section dependence on μ_R is much larger than on μ_F . At NLO the situation is slightly different, because the dependence of the cross section on μ_F increases substantially. However, σ^{NLO} is still dominated by the changes in μ_R .

4.2 Differential distributions

An important task of studies on higher-order corrections is to examine how much they can affect the shape of various kinematic distributions. It is equally important to estimate the final theoretical error for differential cross sections. In the following we shall examine various observables that are of interest for the LHC. For the default PDF set we plot each observable twice, once for $\mu_0 = m_t + m_W/2$ and once for $\mu_0 = H_T/3$. The upper panel of each plot shows the absolute prediction at LO and NLO together with their scale dependence bands calculated according to Eq. (3.8). The lower panels display the same LO and NLO predictions normalised to the LO result at $\mu_R = \mu_F = \mu_0$. The blue band provides the relative scale uncertainty of the LO cross section, whereas the red band gives the differential \mathcal{K} -factor together with its uncertainty band. We have examined about 30 observables. In the following we shall present, however, just a few examples to highlight the main features and importance of higher-order QCD corrections for the $pp \rightarrow e^+ \nu_e \mu^- \bar{\nu}_\mu e^+ \nu_e b \bar{b} + X$ process.

We start with the scalar sum of the transverse momenta of the charged leptons available in this process, which we label H_T^{lep} and define as

$$H_T^{lep} = p_T(\mu^-) + p_T(\ell_1) + p_T(\ell_2), \quad (4.7)$$

where $\ell_{1,2} = e_{1,2}^+$. Also examined is the scalar sum of the transverse momenta of the visible final states denoted as H_T^{vis} and given by

$$H_T^{vis} = p_T(\mu^-) + p_T(\ell_1) + p_T(\ell_2) + p_T(j_{b_1}) + p_T(j_{b_2}). \quad (4.8)$$

Both observables, which are often exploited in various SM measurements and BSM searches by the ATLAS and CMS collaborations, are displayed in Figure 5. We examine first the size of NLO QCD corrections. With the fixed scale choice higher-order corrections from about +25% at the begin of the spectrum down to about -35% for the high p_T tails can be observed for H_T^{lep} causing distortions up to 60%. For the dynamical scale choice, on the other hand, NLO QCD corrections are up to about $\pm 10\%$ only, leading to maximal distortions of the order of 20%. Still, independently of the scale choice the H_T^{lep} differential \mathcal{K} -factor is not flat highlighting the importance of NLO QCD corrections. A very similar conclusion could be drawn for the second observable H_T^{vis} . Furthermore, alike for the H_T^{lep} and H_T^{vis} observables with the fixed scale choice the NLO error bands do not fit within the LO ones. A scale variation procedure is considered good only if the error estimate at the LO contains the central value of the next higher order, see e.g. [83], which is not the case here. Thus, $\mu_0 = m_t + m_W/2$ leads to perturbative instabilities in the TeV region of the differential cross section distributions. The dynamical scale choice, however, stabilises the tails and keeps the NLO uncertainties bands within the LO ones as one would expect from a well behaved perturbative expansion. As for the theoretical uncertainties due to the scale dependence also at the differential level we notice a substantial reduction of the uncertainties when the higher-order QCD corrections are incorporated. For both observables theoretical uncertainties for the fixed scale choice are maximally up to 15% – 20%, whereas for the dynamical scale choice they are of the order of 5% – 10%.

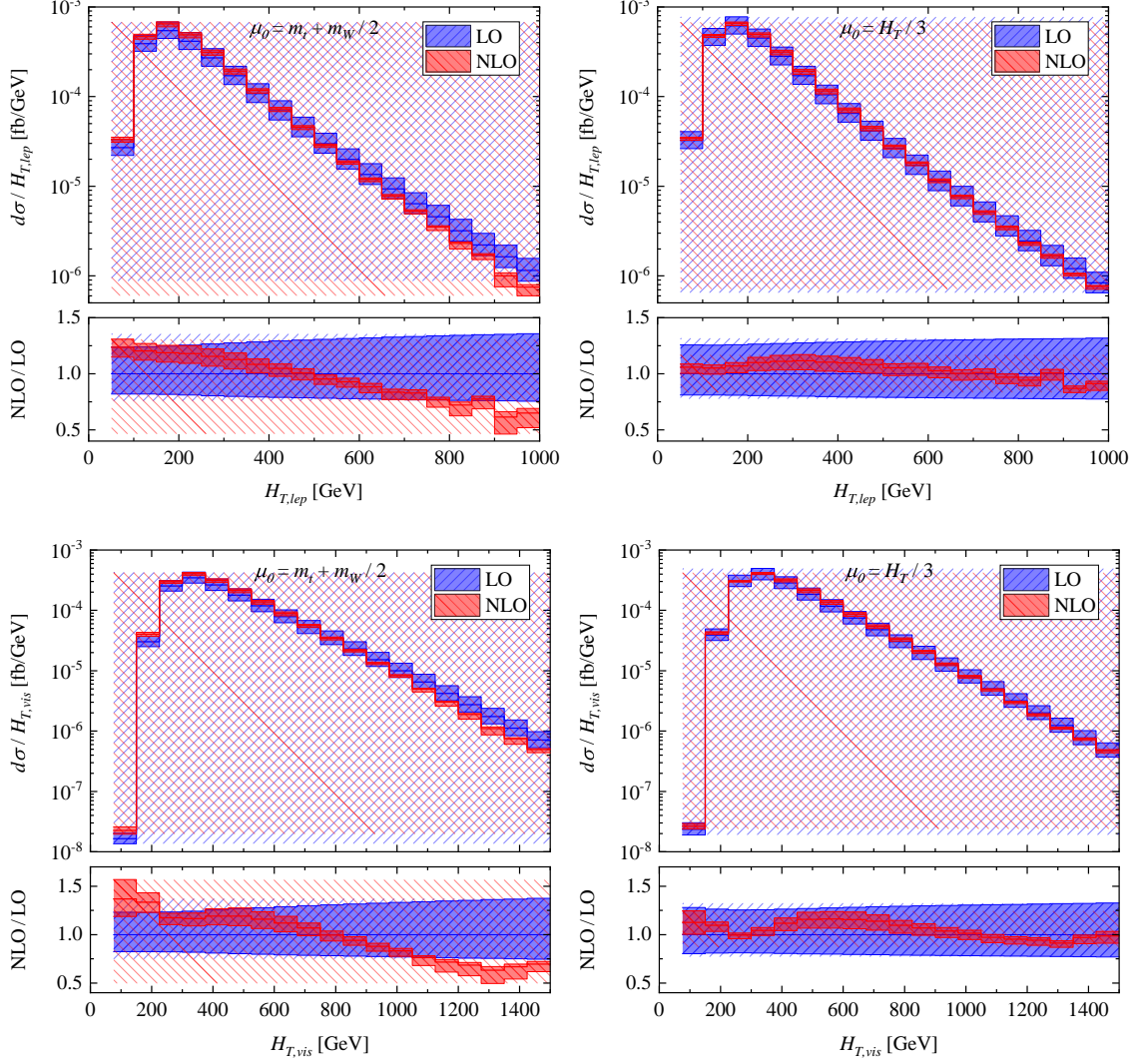


Figure 5. The $pp \rightarrow e^+ \nu_e \mu^- \bar{\nu}_\mu e^+ \nu_e b \bar{b} + X$ differential cross section distribution at the LHC with $\sqrt{s} = 13$ TeV as a function of H_T^{lep} and H_T^{vis} . The upper panels show absolute LO and NLO predictions together with corresponding uncertainty bands. The lower panels display the differential \mathcal{K} -factor together with the uncertainty band and the relative scale uncertainties of the LO cross section. Results are evaluated using $\mu_R = \mu_F = \mu_0$ with $\mu_0 = m_t + m_W/2$ and $\mu_0 = H_T/3$. The LO and the NLO NNPDF3.0 PDF sets are employed.

In the next step we present the transverse momentum distribution of the hardest positron, denoted as p_{T,e_1} , and the invariant mass of the hardest positron and the muon, labeled as $M_{e_1\mu^-}$. Both observables are depicted in Figure 6. For the p_{T,e_1} differential cross section distribution with $\mu_0 = m_t + m_W/2$ NLO QCD corrections in the range from +25% to -15% are obtained. Once the kinematic dependent scale choice is used instead we have rather constant positive corrections of the order of 10%. Also here similar results are observed for the $M_{e_1\mu^-}$ differential cross section distribution. The resulting uncertainties

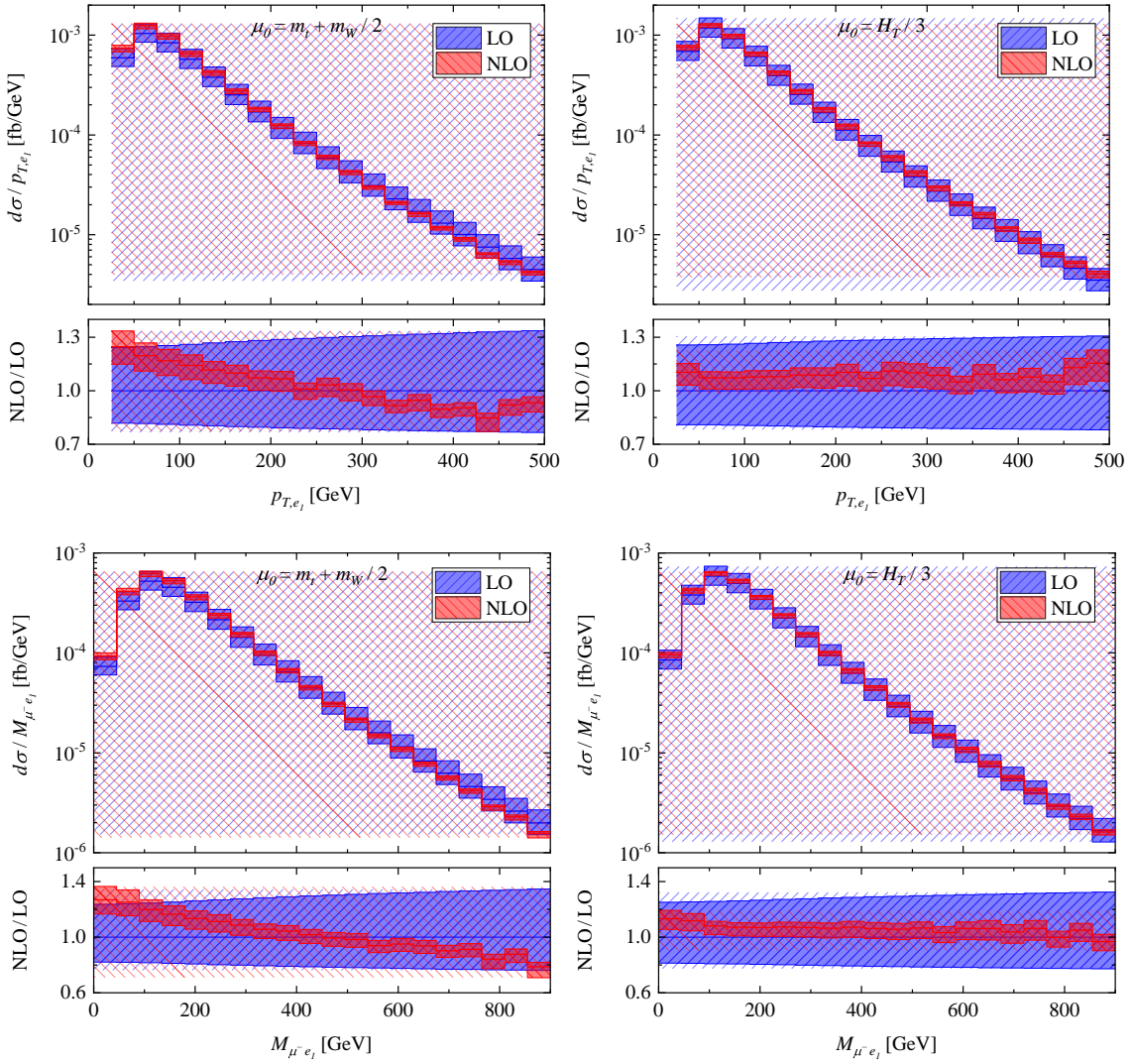


Figure 6. As in Figure 5 but for the p_{T,e_1} and $M_{\mu^-e_1}$ distributions.

for both observables are below 10% independently of the chosen scale.

Finally, in Figure 7 we show the rapidity of the hardest positron, y_{e_1} , and the separation in the rapidity-azimuthal angle plane between the muon and the hardest positron, $\Delta R_{\mu^-e_1}$. Using $\mu_0 = m_t + m_W/2$ for y_{e_1} we receive positive 10% – 20% NLO QCD corrections in the central rapidity regions. When approaching the forward and backward regions of the detector these corrections increase rapidly up to even 45%. The situation is once again improved by the dynamical scale choice. In the central rapidity regions higher-order corrections are only up to 10% whereas for the forward and backward regions they increase to 30% – 35%. Theoretical uncertainties follow the same pattern. They are rather small for $|y_{e_1}| < 1.5$ of the order of 5% – 10% and moderate, up to 20%, for $|y_{e_1}| \in (1.5 - 2.5)$ independently of the scale choice. Similar conclusions can be drawn in the case of $\Delta R_{\mu^-e_1}$.

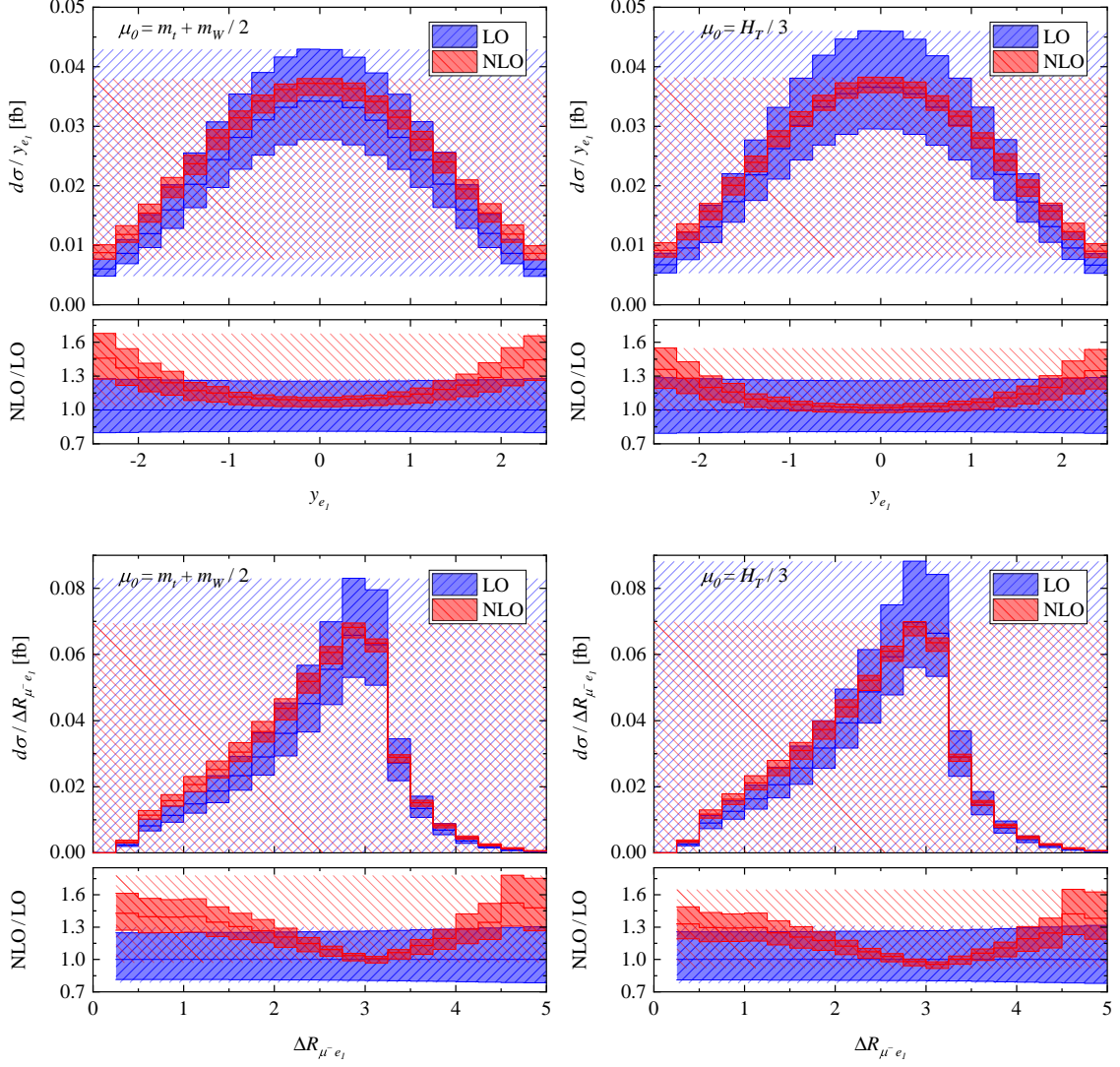


Figure 7. As in Figure 5 but for the y_{e_1} and $\Delta R_{\mu^- e_1}$ distributions.

For both observables the differential \mathcal{K} -factors have large variations.

Overall, the introduction of the dynamical scale stabilises the high p_T tails of various dimensionful observables and generally provides smaller NLO QCD corrections as well as theoretical uncertainties. We observe NLO QCD effects up to 10%–20% and the theoretical uncertainties due to scale dependence below 10%. For various dimensionless (angular) cross section distributions the situation is similar in the central rapidity regions of the detector. Higher order effects are amplified once the more forward and backward regions are examined instead. Independently, in many cases that we have examined, the differential \mathcal{K} -factors are far from flat curves, which implies that the NLO QCD corrections have to be always taken into account to properly model the kinematics of the process.

4.3 PDF uncertainties

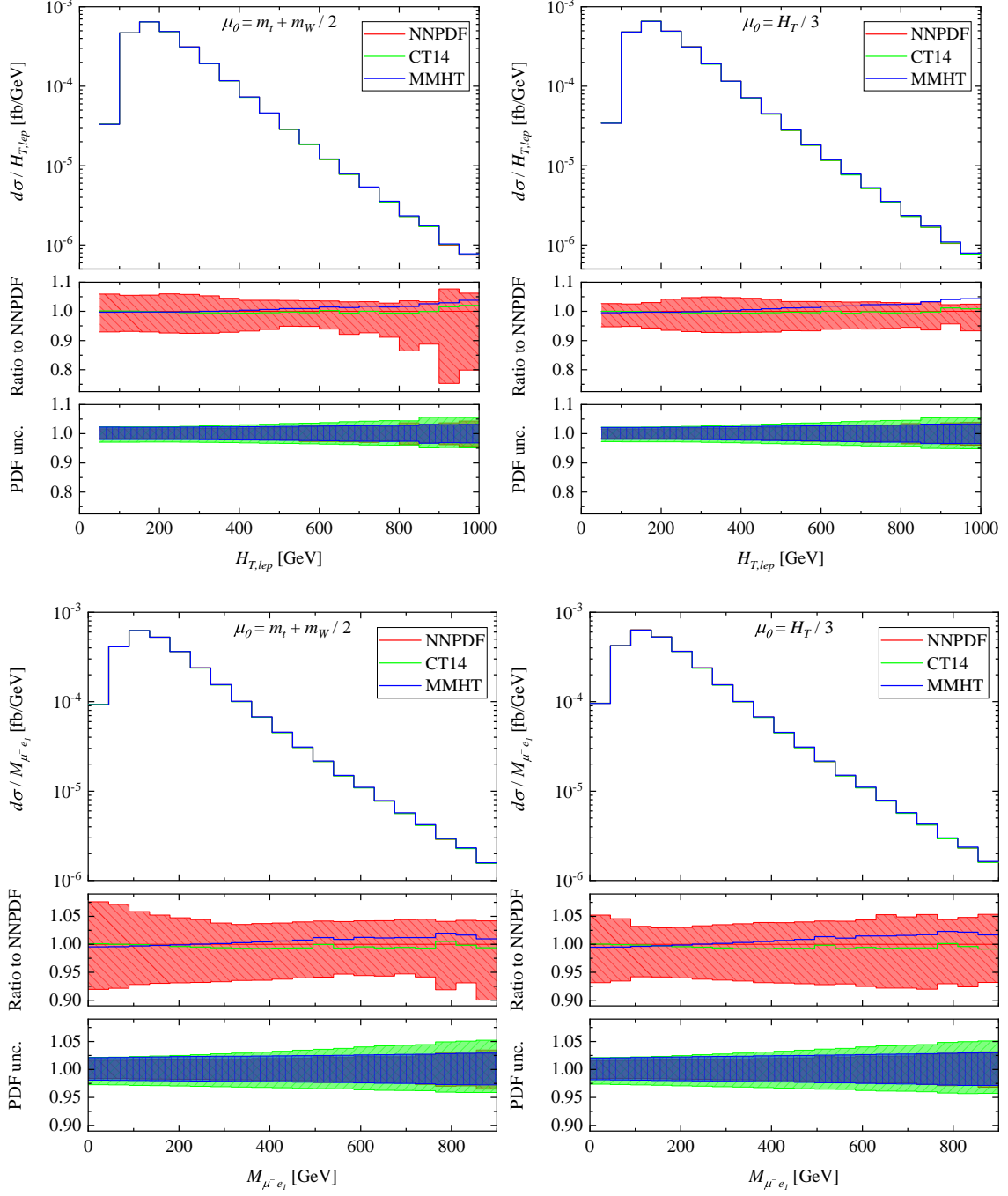


Figure 8. Differential cross section distributions for the $pp \rightarrow e^+ \nu_e \mu^- \bar{\nu}_\mu e^+ \nu_e b \bar{b} + X$ process at the LHC with $\sqrt{s} = 13$ TeV as a function of H_T^{lep} and $M_{\mu^- e_1}$. The upper plot shows the absolute NLO QCD predictions for three different PDF sets with $\mu_R = \mu_F = \mu_0$. The middle panel displays the ratio to the result with the default NNPDF3.0 PDF set as well as its scale dependence. The lower panel presents the internal PDF uncertainties calculated separately for each PDF set.

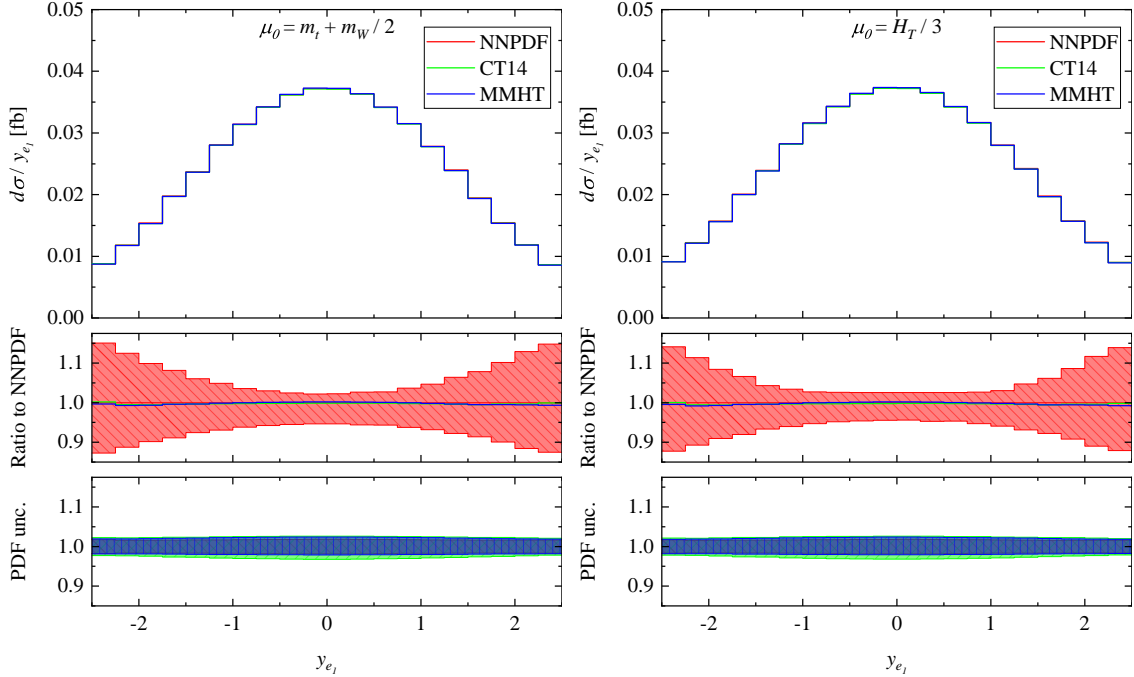


Figure 9. As in Figure 8 but for the y_{e_1} distribution.

To fully assess the theoretical uncertainties inherent in our predictions, we shall examine the PDF uncertainties at the differential level. We have already checked that the latter are below the uncertainties stemming from scale variation for the integrated fiducial cross sections. We would like to confirm these findings differentially for a few observables. We concentrate on three differential cross section distributions already shown in the previous section, namely H_T^{lep} , p_{T,e_1} and y_{e_1} . We plot them afresh for three different PDF sets, CT14, MMHT14 and NNPDF3.0. Each plot consists of three parts. The upper panel shows the absolute NLO prediction for three different PDF sets at the central scale value, μ_0 . The middle panel displays the NLO scale dependence band normalised to the NLO prediction for μ_0 and the default NNPDF3.0 PDF set. Also shown is the ratio of NLO QCD predictions generated for the CT14 and MMHT14 PDF set to NNPDF3.0. The lower panel gives the internal PDF uncertainties for each PDF set separately, normalised to the corresponding NLO prediction as obtained with $\mu_R = \mu_F = \mu_0$.

We begin with the differential cross section distribution as a function of H_T^{lep} shown in Figure 8. For the fixed scale choice the PDF uncertainties are of the order of 5%, thus, negligible when contrasted with the theoretical uncertainties from the scale dependence. Additionally, the differences between results obtained for various PDF sets are similar in size to the internal PDF uncertainties. For the dynamical scale choice the PDF uncertainties and the scale dependence can be of a similar size, especially in the high p_T regions of the phase space.

For the invariant mass of the muon and the hardest positron, also given in Figure 8,

the PDF uncertainties are again only up to 5%. Thus, they are smaller than the scale dependence in the whole plotted range independently of the scale choice.

Finally, the dominance of the scale dependence is even more pronounced for the rapidity distribution of the hardest positron, presented in Figure 9. In this case the PDF uncertainties are well below 3%, therefore, completely negligible when compared with theoretical uncertainties due to the scale dependence. Moreover, the differences between various PDF sets at the central scale value, μ_0 , are insignificant. These findings are independent of the scale choice.

To summarise this part, apart from the high p_T phase space regions for a few observables the theoretical uncertainties due to the scale dependence are the dominant source of the theoretical systematics also for the differential cross sections distributions at NLO in QCD.

4.4 Off-shell versus on-shell top quark decay modelling

In this part of the paper we shall examine the size of the non-factorisable corrections for the $pp \rightarrow e^+ \nu_e \mu^- \bar{\nu}_\mu e^+ \nu_e b\bar{b} + X$ process within our setup. The non-factorisable corrections vanish in the limit $\Gamma_t/m_t \rightarrow 0$, which characterises the NWA. Therefore, to inspect them closely we compare the NLO QCD results with the complete top-quark off-shell effects included with the calculations in the NWA. The latter results are also generated with the help of the HELAC-NLO MC program, that has recently been extended to provide theoretical predictions in this approximation [84]. The NWA results are divided in two categories: the full NWA and the $\text{NWA}_{\text{LOdecay}}$. The full NWA comprises NLO QCD corrections to both the $t\bar{t}W^\pm$ production and the subsequent top-quark decays preserving at the same time the $t\bar{t}$ spin correlations. The $\text{NWA}_{\text{LOdecay}}$ case contains the results with NLO QCD corrections to the production stage only, whereas the top-quark decays are calculated at LO. For consistency the NWA result with the LO top-quark decays is calculated with $\Gamma_{t,\text{NWA}}^{\text{LO}}$. The LO and NLO theoretical predictions for the three cases are listed in Table 4. Also provided are the theoretical uncertainties due to scale dependence. All results are evaluated for the default NNPDF3.0 PDF sets. To ensure consistency in the comparison the unexpanded NWA results are used ². We have checked, however, that the expanded results are slightly smaller. The difference between the expanded and unexpanded NWA results is at 3% level for $\mu_0 = H_T/3$ and around 4% for $\mu_0 = m_t + m_W/2$.

For the $pp \rightarrow e^+ \nu_e \mu^- \bar{\nu}_\mu e^+ \nu_e b\bar{b} + X$ process the complete top-quark off-shell effects change the integrated NLO fiducial cross section by less than 0.2% independent of the scale choice. The finding is consistent with the expected uncertainty of the NWA [85], which is of the order of $\mathcal{O}(\Gamma_t/m_t) \approx 0.8\%$ for the inclusive observables. Having the results in the $\text{NWA}_{\text{LOdecay}}$ to our disposal we can additionally observe that the NLO QCD corrections to top-quark decays are negative and at the level of 3% for the fixed scale choice. They increase up to 5% when the dynamical scale is used instead. Also provided in Table 4 are the theoretical uncertainties due to scale dependence. They are given for all three cases to help us to investigate whether theoretical uncertainties are underestimated when

² For consistency in the NWA result the top quark width Γ_t^{NLO} , which appears in $\sigma_{t\bar{t}W^\pm}^{\text{NLO}}$ as the factor $(\Gamma_t^{\text{NLO}})^{-2}$, should also be computed in series of α_s . In our NLO results in the NWA, however, the top quark width is not expanded since this procedure can not be directly applied to the full off-shell calculation.

MODELLING APPROACH	σ^{LO} [ab]	σ^{NLO} [ab]
full off-shell ($\mu_0 = m_t + m_W/2$)	106.9 ^{+27.7 (26%)} -20.5 (19%)	123.2 ^{+6.3 (5%)} -8.7 (7%)
full off-shell ($\mu_0 = H_T/3$)	115.1 ^{+30.5 (26%)} -22.5 (20%)	124.4 ^{+4.3 (3%)} -7.7 (6%)
NWA ($\mu_0 = m_t + m_W/2$)	106.4 ^{+27.5 (26%)} -20.3 (19%)	123.0 ^{+6.3 (5%)} -8.7 (7%)
NWA ($\mu_0 = H_T/3$)	115.1 ^{+30.4 (26%)} -22.4 (19%)	124.2 ^{+4.1 (3%)} -7.7 (6%)
NWA _{LOdecay} ($\mu_0 = m_t + m_W/2$)		127.0 ^{+14.2 (11%)} -13.3 (10%)
NWA _{LOdecay} ($\mu_0 = H_T/3$)		130.7 ^{+13.6 (10%)} -13.2 (10%)

Table 4. Integrated fiducial cross sections for the $pp \rightarrow e^+ \nu_e \mu^- \bar{\nu}_\mu e^+ \nu_e b\bar{b} + X$ process at the LHC with $\sqrt{s} = 13$ TeV. Results for various approaches for the modelling of top quark production and decays are listed. Theoretical uncertainties as obtained from the scale dependence are also provided. The NNPDF3.0 PDF sets are employed.

various approximations for the top-quark production and decays are employed instead of the full description. When comparing the full off-shell case with the full NWA we notice that theoretical uncertainties are similar, consistently below 6% – 7% independently of the scale choice. For the NWA_{LOdecay} case, however, they rise up to 10% – 11%. We observe that adding NLO QCD corrections to decays compensates part of the scale dependence of the cross section with the corrections in the production.

In summary, both the complete top-quark off-shell effects and the NLO QCD corrections to top-quark decays are rather small for the integrated fiducial cross sections. They are consistently within the NLO theoretical uncertainty estimates for the $pp \rightarrow e^+ \nu_e \mu^- \bar{\nu}_\mu e^+ \nu_e b\bar{b} + X$. Additionally, we note that the full NWA results match better the complete off-shell predictions on a scale-by-scale basis. Regardless of the considerations on the scale dependence reduction, the theoretical description of $t\bar{t}W^\pm$ can only benefit from a more accurate modelling of top-quark decays.

A completely different picture emerges when various differential (fiducial) cross section distributions are analysed at the NLO level in QCD. In Figure 10 we exhibit H_T^{vis} and H_T . The latter is defined in Eq. (3.11). Also shown in Figure 10 are the invariant mass of the two b -jets, $M_{b_1 b_2}$, and the transverse momentum of the hardest b -jet, p_{T, b_1} . The same three theoretical descriptions, i.e. the full NWA, the NWA_{LOdecay} and the full off-shell case, are plotted for the dynamical scale choice and the default NNPDF3.0 PDF set. We refrain from presenting differential results for $\mu_0 = m_t + m_W/2$ because, as we have seen, this scale choice is not appropriate for differential description of the $pp \rightarrow e^+ \nu_e \mu^- \bar{\nu}_\mu e^+ \nu_e b\bar{b} + X$

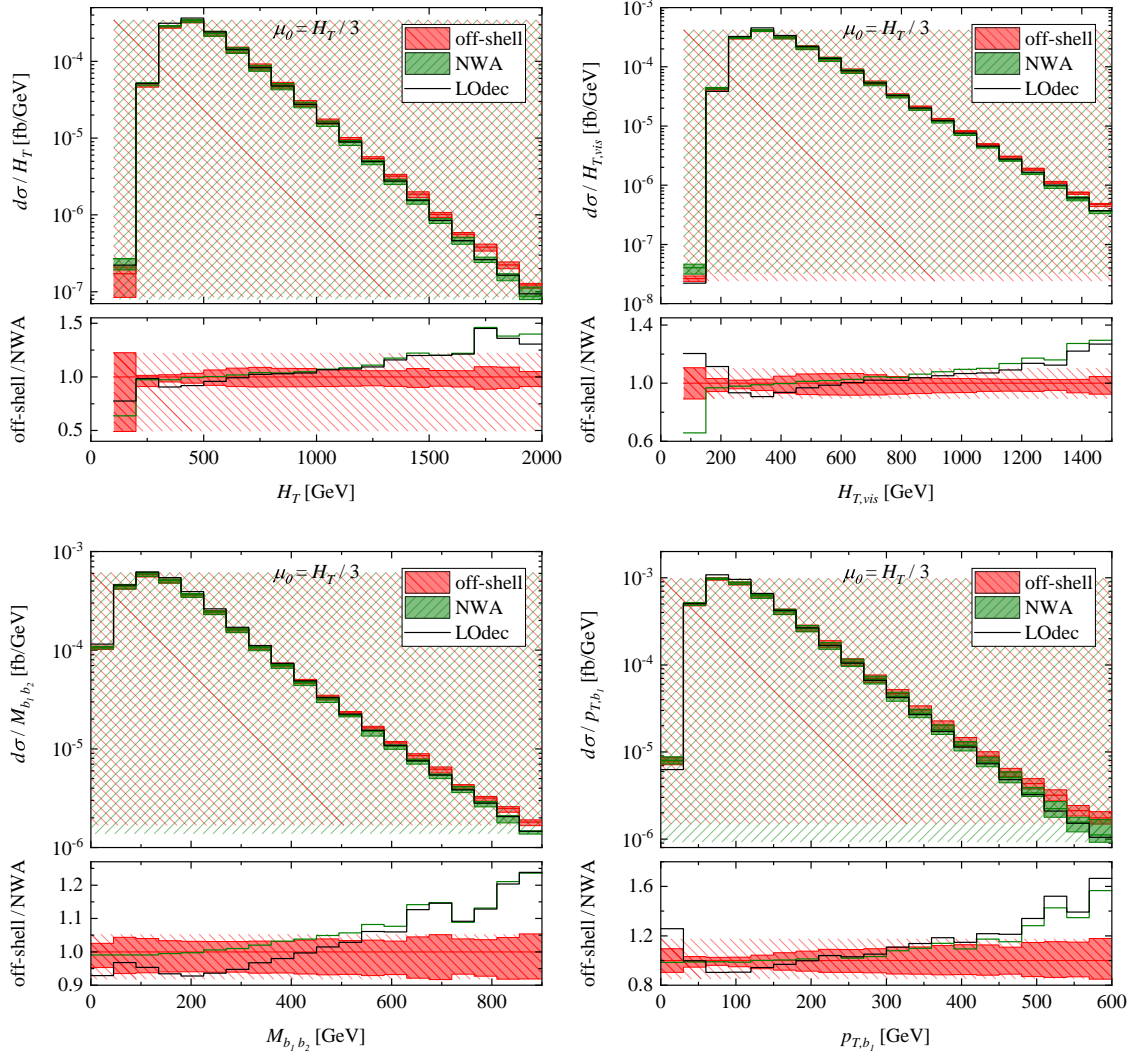


Figure 10. Differential cross section distribution as a function of H_T , H_T^{vis} , $M(b_1 b_2)$ and $p_T(b_1)$ for the $pp \rightarrow e^+ \nu_e \mu^- \bar{\nu}_\mu e^+ \nu_e b \bar{b} + X$ production process at the LHC with $\sqrt{s} = 13$ TeV. NLO QCD results for various approaches for the modelling of top quark production and decays are shown. We additionally provide theoretical uncertainties as obtained from the scale dependence for the full off-shell case. Also plotted are the ratios of the full off-shell result to the two NWA results. The NNPDF3.0 PDF sets is employed.

process. For the full off-shell case we additionally display the theoretical uncertainties as obtained from the scale dependence since we are interested in effects that are outside the NLO uncertainties bands. The upper plots show the absolute predictions at NLO in QCD, whereas the bottom plots exhibit the ratios of the full off-shell result to the two NWA results.

At the tails of the H_T^{vis} distribution we observe that top-quark off-shell effects increase up to 30%. This is well above the theoretical uncertainties due to scale dependence that for a majority of dimensionful observables are around $\pm 10\%$. Furthermore, at the beginning

of the spectrum above the kinematical cutoff of $H_T^{vis} \approx 125$ GeV we can notice large discrepancies between the full NWA description and the $NWA_{LOdecay}$ case. They are visible up to about 400 GeV, thus, in the regions that are currently scrutinised by the ATLAS and CMS experiments. Also in this region of the H_T^{vis} differential cross section distribution the top-quark off-shell effects are substantial, of the order of 20% – 35%. Similar conclusions can be drawn for H_T . In the following we examine the kinematics of the b -jets. For the invariant mass of two b -jets the top-quark off-shell effects are up to 25%, whereas in the case of the transverse momentum of the hardest b -jet they are as large as 60% – 70%. For the small values of $M_{b_1 b_2}$ and p_{T, b_1} we can notice 10% – 25% effects. For the central value of the scale substantial differences between the full NWA description and the $NWA_{LOdecay}$ case are visible also for these two observables. This highlights the importance of the proper modelling of top-quark decays for this process.

In conclusion, in the case of various (dimensionful) differential cross sections, non-negligible top-quark off-shell effects are present in various phase-space regions. Substantial differences between the two versions of the NWA results are additionally observed. Taking into account that a priori it is not possible to estimate the size of these effects and which phase space regions are particularly affected a very careful examination based on the full theoretical description should be performed on a case-by-case basis. For that reason the complete top-quark off-shell effects should be included at the differential level in future comparisons between theoretical predictions and experimental data.

5 Phenomenological results for $t\bar{t}W^-$

In this section we would like to present the results for the $t\bar{t}W^-$ process with the complete top quark and W gauge boson off-shell effects included. As mentioned in the introduction, however, only theoretical predictions for the integrated fiducial cross section will be shown. The main reason is not to extend the manuscript length unnecessarily taking into account that the NLO QCD effects for $t\bar{t}W^+$ and $t\bar{t}W^-$ are very similar.

With the input parameters and cuts specified before, we arrive at the following predictions for the $pp \rightarrow e^- \bar{\nu}_e \mu^+ \nu_\mu e^- \bar{\nu}_e b\bar{b} + X$ process using the default NNPDF3.0 PDF sets and the fixed scale choice

$$\begin{aligned} \sigma_{e^- \bar{\nu}_e \mu^+ \nu_\mu e^- \bar{\nu}_e b\bar{b}}^{LO}(\text{NNPDF3.0}, \mu_0 = m_t + m_W/2) &= 57.2_{-11.0}^{+14.9} (26\%) [\text{scale}] \text{ ab}, \\ \sigma_{e^- \bar{\nu}_e \mu^+ \nu_\mu e^- \bar{\nu}_e b\bar{b}}^{NLO}(\text{NNPDF3.0}, \mu_0 = m_t + m_W/2) &= 68.0_{-5.5}^{+4.8} (7\%) [\text{scale}]_{-1.2}^{+1.2} (2\%) [\text{PDF}] \text{ ab}. \end{aligned} \tag{5.1}$$

When the MMHT14 PDF sets are employed instead the following results are reported

$$\begin{aligned} \sigma_{e^- \bar{\nu}_e \mu^+ \nu_\mu e^- \bar{\nu}_e b\bar{b}}^{LO}(\text{MMHT14}, \mu_0 = m_t + m_W/2) &= 55.6_{-10.7}^{+14.5} (26\%) [\text{scale}] \text{ ab}, \\ \sigma_{e^- \bar{\nu}_e \mu^+ \nu_\mu e^- \bar{\nu}_e b\bar{b}}^{NLO}(\text{MMHT14}, \mu_0 = m_t + m_W/2) &= 68.3_{-5.4}^{+4.6} (7\%) [\text{scale}]_{-1.4}^{+1.6} (2\%) [\text{PDF}] \text{ ab}. \end{aligned} \tag{5.2}$$

MODELLING APPROACH	σ^{LO} [ab]	σ^{NLO} [ab]
full off-shell ($\mu_0 = m_t + m_W/2$)	$57.2^{+14.9(26\%)}_{-11.0(19\%)}$	$68.0^{+4.8(7\%)}_{-5.5(8\%)}$
full off-shell ($\mu_0 = H_T/3$)	$62.4^{+16.7(27\%)}_{-12.3(20\%)}$	$68.6^{+3.5(5\%)}_{-4.8(7\%)}$
NWA ($\mu_0 = m_t + m_W/2$)	$57.2^{+14.9(26\%)}_{-11.0(19\%)}$	$68.0^{+4.9(7\%)}_{-5.4(8\%)}$
NWA ($\mu_0 = H_T/3$)	$62.6^{+16.7(27\%)}_{-12.3(20\%)}$	$68.7^{+3.5(5\%)}_{-4.8(7\%)}$
NWA _{LOdecay} ($\mu_0 = m_t + m_W/2$)		$69.8^{+8.8(13\%)}_{-7.8(11\%)}$
NWA _{LOdecay} ($\mu_0 = H_T/3$)		$72.0^{+8.3(11\%)}_{-7.7(11\%)}$

Table 5. Integrated fiducial cross sections for the $pp \rightarrow e^- \bar{\nu}_e \mu^+ \nu_\mu e^- \bar{\nu}_e b \bar{b} + X$ process at the LHC with $\sqrt{s} = 13$ TeV. Results for various approaches for the modelling of top quark production and decays are listed. Theoretical uncertainties as obtained from the scale dependence are also provided. The NNPDF3.0 PDF sets are employed.

Theoretical predictions for the CT14 PDF sets are given by

$$\begin{aligned} \sigma_{e^- \bar{\nu}_e \mu^+ \nu_\mu e^- \bar{\nu}_e b \bar{b}}^{\text{LO}}(\text{CT14}, \mu_0 = m_t + m_W/2) &= 52.4^{+13.4(26\%)}_{-9.9(19\%)} [\text{scale}] \text{ ab}, \\ \sigma_{e^- \bar{\nu}_e \mu^+ \nu_\mu e^- \bar{\nu}_e b \bar{b}}^{\text{NLO}}(\text{CT14}, \mu_0 = m_t + m_W/2) &= 66.7^{+4.4(7\%)}_{-5.3(8\%)} [\text{scale}]^{+1.7(3\%)}_{-2.3(4\%)} [\text{PDF}] \text{ ab}. \end{aligned} \quad (5.3)$$

The integrated fiducial cross section for $pp \rightarrow e^- \bar{\nu}_e \mu^+ \nu_\mu e^- \bar{\nu}_e b \bar{b} + X$ is about a factor of two smaller than the one for the $pp \rightarrow e^+ \nu_e \mu^- \bar{\nu}_\mu e^+ \nu_e b \bar{b} + X$ process. On the other hand, the behaviour of the QCD higher-order corrections is rather similar for both processes as one would expect since they are highly correlated. Specifically, the NLO QCD corrections are positive and moderate of the order of 19% for the default NNPDF3.0 set. They increase up to 23% (27%) for MMHT14 (CT14). The size of theoretical uncertainties due to scale variation and PDFs is alike. Also in this case the stability test with respect to the $p_T(j_b)$ cut has been performed for the integrated fiducial cross section yielding excellent theoretical control over higher-order QCD corrections for this process. For completeness we report on the results for the dynamical scale choice, $\mu_0 = H_T/3$, with H_T given this time by

$$H_T = p_T(\ell_1) + p_T(\ell_2) + p_T(\mu^+) + p_T^{\text{miss}} + p_T(j_{b_1}) + p_T(j_{b_2}), \quad (5.4)$$

where $\ell_{1,2} = e_{1,2}^-$ are the hardest and the softest electron. For the NNPDF3.0 PDF sets we have

$$\begin{aligned} \sigma_{e^- \bar{\nu}_e \mu^+ \nu_\mu e^- \bar{\nu}_e b \bar{b}}^{\text{LO}}(\text{NNPDF3.0}, \mu_0 = H_T/3) &= 62.4^{+16.7(27\%)}_{-12.3(20\%)} [\text{scale}] \text{ ab}, \\ \sigma_{e^- \bar{\nu}_e \mu^+ \nu_\mu e^- \bar{\nu}_e b \bar{b}}^{\text{NLO}}(\text{NNPDF3.0}, \mu_0 = H_T/3) &= 68.6^{+3.5(5\%)}_{-4.8(7\%)} [\text{scale}]^{+1.2(2\%)}_{-1.2(2\%)} [\text{PDF}] \text{ ab}. \end{aligned} \quad (5.5)$$

For the MMHT14 PDF sets the results are as follows

$$\begin{aligned}\sigma_{e^-\bar{\nu}_e\mu^+\nu_\mu e^-\bar{\nu}_e b\bar{b}}^{\text{LO}}(\text{MMHT14}, \mu_0 = H_T/3) &= 60.5_{-11.9(20\%)}^{+16.1(27\%)} [\text{scale}] \text{ ab}, \\ \sigma_{e^-\bar{\nu}_e\mu^+\nu_\mu e^-\bar{\nu}_e b\bar{b}}^{\text{NLO}}(\text{MMHT14}, \mu_0 = H_T/3) &= 68.9_{-4.7(7\%)}^{+3.3(5\%)} [\text{scale}]_{-1.4(2\%)}^{+1.6(2\%)} [\text{PDF}] \text{ ab}.\end{aligned}\tag{5.6}$$

With the CT14 PDF sets the results read

$$\begin{aligned}\sigma_{e^-\bar{\nu}_e\mu^+\nu_\mu e^-\bar{\nu}_e b\bar{b}}^{\text{LO}}(\text{CT14}, \mu_0 = H_T/3) &= 57.0_{-11.0(19\%)}^{+14.9(26\%)} [\text{scale}] \text{ ab}, \\ \sigma_{e^-\bar{\nu}_e\mu^+\nu_\mu e^-\bar{\nu}_e b\bar{b}}^{\text{NLO}}(\text{CT14}, \mu_0 = H_T/3) &= 67.3_{-4.6(7\%)}^{+3.1(5\%)} [\text{scale}]_{-2.3(3\%)}^{+1.7(3\%)} [\text{PDF}] \text{ ab}.\end{aligned}\tag{5.7}$$

Finally, in Table 5 we present the integrated fiducial cross sections for the full off-shell case, the full NWA and for $\text{NWA}_{\text{LOdecay}}$. Theoretical uncertainties as obtained from scale variations are also provided. All LO and NLO results are presented for the default NNPDF3.0 PDF sets. Our findings are much the same as in the case of the $pp \rightarrow e^+\nu_e\mu^-\bar{\nu}_e e^+\nu_e b\bar{b} + X$ production process.

6 Summary and Outlook

In this paper we have calculated NLO QCD corrections to the $e^+\nu_e\mu^-\bar{\nu}_e e^+\nu_e b\bar{b}$ and $e^-\bar{\nu}_e\mu^+\nu_\mu e^-\bar{\nu}_e b\bar{b}$ final states in $t\bar{t}W^\pm$ production. In the computation off-shell top quarks have been described by the Breit-Wigner distribution, furthermore double-, single- as well as non-resonant top quark contributions along with all interference effects have been consistently incorporated already at the matrix element level. We presented our results for the LHC Run II centre of mass system energy of $\sqrt{s} = 13$ TeV for the two scale choices $\mu_0 = m_t + m_W/2$ and $\mu_0 = H_T/3$ and the following three PDF sets NNPDF3.0, MMHT14 and CT14. For the default NNPDF3.0 PDF set with $\mu_0 = m_t + m_W/2$ moderate NLO QCD corrections of the order of 15% (19%) have been found for the $t\bar{t}W^+$ ($t\bar{t}W^-$) integrated fiducial cross section. When $\mu_0 = H_T/3$ has been employed instead they are reduced down to 8% (10%) respectively. Detailed studies of the scale dependence of our NLO predictions have indicated that the residual theoretical uncertainties due to missing higher-order corrections are below 6% – 8% independently of the scale choice. The PDF uncertainties are up to 2% – 4% only. Thus, the theoretical uncertainties due to the scale dependence are the dominant source of the theoretical systematics.

For differential cross section distributions large shape distortions have been observed in the presence of higher-order QCD effects. The non-flat differential \mathcal{K} -factors underlined the importance of NLO QCD corrections for proper modelling of the process kinematics. Furthermore, we observed that $\mu_0 = m_t + m_W/2$ led to perturbative instabilities in the TeV regions of various dimensionful observables. The introduction of the dynamical scale stabilised the high p_T tails and generally provided smaller NLO QCD corrections as well as theoretical uncertainties. For $\mu_0 = H_T/3$ we obtained NLO QCD effects up to 10% – 20% and the theoretical uncertainties due to scale dependence are below 10%. The latter are the dominant source of the theoretical systematics.

In addition, the size of the complete top-quark off-shell effects has been examined. For the integrated fiducial cross sections negligible effects, that are consistent with the expected uncertainty of the NWA, have been found. At the differential level, however, large non-factorisable corrections even up to 60% – 70% have been observed.

Last but not least, the size of NLO QCD corrections to the top-quark decays has been studied. These corrections were rather small up to 5% only for the integrated fiducial cross sections. For various differential distributions, on the other hand, the differences between the full NWA and the $\text{NWA}_{\text{LOdecay}}$ case were substantial especially in the low p_T regions. The latter phase space regions are currently scrutinised by the ATLAS and CMS experimental collaborations at the LHC. Furthermore, for the integrated fiducial cross section we noticed that the theoretical uncertainties due to scale dependence were alike for the full off-shell and full NWA case. They were systematically below 6% – 8% showing that the full NWA predictions would not underestimate or overestimate the theoretical uncertainties as long as NLO QCD corrections were consistently incorporated at every stage of the process. Having rather small uncertainties for the $t\bar{t}W^\pm$ process force us to look for other effects, that might be of comparable size. The latter, comprise for example formally sub-leading electroweak corrections, which include $tW \rightarrow tW$ scattering [34]. As shown in Ref. [34] the combined effect of spin correlations in the top-quark pair and sub-leading electroweak contributions, which were larger than the so-called NLO electroweak corrections, would enhance the normalisation of the $t\bar{t}W$ process by approximately 10%.

Finally, in the case of $\text{NWA}_{\text{LOdecay}}$, i.e. in the presence of LO top-quark decays, theoretical uncertainties at NLO in QCD increased to 11% – 13%. Regardless of the considerations on the scale dependence reduction, the theoretical description of $t\bar{t}W^\pm$ can only benefit from a more accurate modelling of top-quark decays.

To recapitulate, the non-factorisable NLO QCD corrections as well as higher-order QCD effects in top-quark decays impacted significantly the $t\bar{t}W^\pm$ cross section in various phase space regions. For these reasons they should both be included in the future comparisons between theoretical predictions and experimental data. In addition, in view of the importance of the $t\bar{t}W^\pm$ process as background to Higgs boson production in association with the top quark pairs, more detailed and combined phenomenological studies for $t\bar{t}W^+$ and $t\bar{t}W^-$ in the multi-lepton channel are a necessity. We postpone such work for the future.

Acknowledgments

The research of G.B. was supported by grant K 125105 of the National Research, Development and Innovation Office in Hungary.

The work of H.B.H. has received funding from the European Research Council (ERC) under the European Union’s Horizon 2020 research and innovation programme (grant agreement No 772099).

The work of H.B. and M.W. was supported by the Deutsche Forschungsgemeinschaft (DFG) under grant 396021762 – TRR 257.

Support by a grant of the Bundesministerium für Bildung und Forschung (BMBF) is additionally acknowledged.

Simulations were performed with computing resources granted by RWTH Aachen University under project `rwth0414`.

References

- [1] M. Aaboud *et al.* [ATLAS Collaboration], *Measurement of the $t\bar{t}Z$ and $t\bar{t}W$ production cross sections in multilepton final states using 3.2 fb^{-1} of pp collisions at $\sqrt{s} = 13\text{ TeV}$ with the ATLAS detector*, Eur. Phys. J. C **77** (2017) no.1, 40 [[arXiv:1609.01599](#) [[hep-ex](#)]].
- [2] A. M. Sirunyan *et al.* [CMS Collaboration], *Measurement of the cross section for top quark pair production in association with a W or Z boson in proton-proton collisions at $\sqrt{s} = 13\text{ TeV}$* , JHEP **1808** (2018) 011 [[arXiv:1711.02547](#) [[hep-ex](#)]].
- [3] The ATLAS collaboration [ATLAS Collaboration], *Analysis of $t\bar{t}H$ and $t\bar{t}W$ production in multilepton final states with the ATLAS detector*, [ATLAS-CONF-2019-045](#).
- [4] M. Aaboud *et al.* [ATLAS Collaboration], *Measurement of the $t\bar{t}Z$ and $t\bar{t}W$ cross sections in proton-proton collisions at $\sqrt{s} = 13\text{ TeV}$ with the ATLAS detector*, Phys. Rev. D **99** (2019) no.7, 072009 [[arXiv:1901.03584](#) [[hep-ex](#)]].
- [5] F. Maltoni, M. L. Mangano, I. Tsinikos and M. Zaro, *Top-quark charge asymmetry and polarization in $t\bar{t}W^\pm$ production at the LHC*, Phys. Lett. B **736** (2014) 252 [[arXiv:1406.3262](#) [[hep-ph](#)]].
- [6] F. Maltoni, D. Pagani and I. Tsinikos, *Associated production of a top-quark pair with vector bosons at NLO in QCD: impact on $t\bar{t}H$ searches at the LHC*, JHEP **1602** (2016) 113 [[arXiv:1507.05640](#) [[hep-ph](#)]].
- [7] A. M. Sirunyan *et al.* [CMS Collaboration], *Observation of $t\bar{t}H$ production*, Phys. Rev. Lett. **120** (2018) no.23, 231801 [[arXiv:1804.02610](#) [[hep-ex](#)]].
- [8] M. Aaboud *et al.* [ATLAS Collaboration], *Observation of Higgs boson production in association with a top quark pair at the LHC with the ATLAS detector*, Phys. Lett. B **784** (2018) 173 [[arXiv:1806.00425](#) [[hep-ex](#)]].
- [9] T. Gleisberg, S. Höche, F. Krauss, M. Schönherr, S. Schumann, F. Siegert and J. Winter, *Event generation with SHERPA 1.1*, JHEP **02** (2009), 007 [[arXiv:0811.4622](#) [[hep-ph](#)]].
- [10] F. Cascioli, P. Maierhöfer and S. Pozzorini, *Scattering Amplitudes with Open Loops*, Phys. Rev. Lett. **108** (2012), 111601 [[arXiv:1111.5206](#) [[hep-ph](#)]].
- [11] J. Alwall *et al.*, *The automated computation of tree-level and next-to-leading order differential cross sections, and their matching to parton shower simulations*, JHEP **1407** (2014) 079 [[arXiv:1405.0301](#) [[hep-ph](#)]].
- [12] G. Aad *et al.* [ATLAS Collaboration], *Search for supersymmetry at $\sqrt{s} = 13\text{ TeV}$ in final states with jets and two same-sign leptons or three leptons with the ATLAS detector*, Eur. Phys. J. C **76** (2016) no.5, 259 [[arXiv:1602.09058](#) [[hep-ex](#)]].
- [13] V. Khachatryan *et al.* [CMS Collaboration], *Search for new physics in same-sign dilepton events in proton-proton collisions at $\sqrt{s} = 13\text{ TeV}$* , Eur. Phys. J. C **76** (2016) no.8, 439 [[arXiv:1605.03171](#) [[hep-ex](#)]].

- [14] A. M. Sirunyan *et al.* [CMS Collaboration], *Search for physics beyond the standard model in events with two leptons of same sign, missing transverse momentum, and jets in proton-proton collisions at $\sqrt{s} = 13$ TeV*, Eur. Phys. J. C **77** (2017) no.9, 578 [[arXiv:1704.07323](#) [[hep-ex](#)]].
- [15] M. Aaboud *et al.* [ATLAS Collaboration], *Search for supersymmetry in final states with two same-sign or three leptons and jets using 36 fb^{-1} of $\sqrt{s} = 13$ TeV pp collision data with the ATLAS detector*, JHEP **1709** (2017) 084 Erratum: [JHEP **1908** (2019) 121] [[arXiv:1706.03731](#) [[hep-ex](#)]].
- [16] R. M. Barnett, J. F. Gunion and H. E. Haber, *Discovering supersymmetry with like sign dileptons*, Phys. Lett. B **315** (1993) 349 [[hep-ph/9306204](#)].
- [17] M. Guchait and D. P. Roy, *Like sign dilepton signature for gluino production at CERN LHC including top quark and Higgs boson effects*, Phys. Rev. D **52** (1995) 133 [[hep-ph/9412329](#)].
- [18] H. Baer, C. h. Chen, F. Paige and X. Tata, *Signals for minimal supergravity at the CERN large hadron collider. 2: Multi - lepton channels*, Phys. Rev. D **53** (1996) 6241 [[hep-ph/9512383](#)].
- [19] H. K. Dreiner, S. Grab, M. Krämer and M. K. Trenkel, *Supersymmetric NLO QCD corrections to resonant slepton production and signals at the Tevatron and the CERN LHC*, Phys. Rev. D **75** (2007) 035003 [[hep-ph/0611195](#)].
- [20] H. C. Cheng, K. T. Matchev and M. Schmaltz, *Bosonic supersymmetry? Getting fooled at the CERN LHC*, Phys. Rev. D **66** (2002) 056006 [[hep-ph/0205314](#)].
- [21] R. Contino and G. Servant, *Discovering the top partners at the LHC using same-sign dilepton final states*, JHEP **0806** (2008) 026 [[arXiv:0801.1679](#) [[hep-ph](#)]].
- [22] J. Maalampi and N. Romanenko, *Single production of doubly charged Higgs bosons at hadron colliders*, Phys. Lett. B **532** (2002) 202 [[hep-ph/0201196](#)].
- [23] F. M. L. Almeida, Jr., Y. do Amaral Coutinho, J. A. Martins Simoes, P. P. Queiroz Filho and C. M. Porto, *Same sign dileptons as a signature for heavy Majorana neutrinos in hadron hadron collisions*, Phys. Lett. B **400** (1997) 331 [[hep-ph/9703441](#)].
- [24] Y. Bai and Z. Han, *Top-antitop and Top-top Resonances in the Dilepton Channel at the CERN LHC*, JHEP **0904** (2009) 056 [[arXiv:0809.4487](#) [[hep-ph](#)]].
- [25] V. Hirschi, R. Frederix, S. Frixione, M. V. Garzelli, F. Maltoni and R. Pittau, *Automation of one-loop QCD corrections*, JHEP **05** (2011), 044 [[arXiv:1103.0621](#) [[hep-ph](#)]].
- [26] M. V. Garzelli, A. Kardos, C. G. Papadopoulos and Z. Trocsanyi, *$t\bar{t}W^\pm$ and $t\bar{t}Z$ Hadroproduction at NLO accuracy in QCD with Parton Shower and Hadronization effects* JHEP **1211** (2012) 056 [[arXiv:1208.2665](#) [[hep-ph](#)]].
- [27] J. M. Campbell and R. K. Ellis, *$t\bar{t}W^\pm$ production and decay at NLO*, JHEP **1207** (2012) 052 [[arXiv:1204.5678](#) [[hep-ph](#)]].
- [28] S. Frixione, V. Hirschi, D. Pagani, H.-S. Shao and M. Zaro, *Electroweak and QCD corrections to top-pair hadroproduction in association with heavy bosons*, JHEP **1506** (2015) 184 [[arXiv:1504.03446](#) [[hep-ph](#)]].
- [29] J. A. Dror, M. Farina, E. Salvioni and J. Serra, *Strong tW Scattering at the LHC*, JHEP **01** (2016), 071 [[arXiv:1511.03674](#) [[hep-ph](#)]].

- [30] R. Frederix, D. Pagani and M. Zaro, *Large NLO corrections in $t\bar{t}W^\pm$ and $t\bar{t}\bar{t}$ hadroproduction from supposedly subleading EW contributions*, JHEP **1802** (2018) 031 [[arXiv:1711.02116](#) [[hep-ph](#)]].
- [31] H. T. Li, C. S. Li and S. A. Li, *Renormalization group improved predictions for $t\bar{t}W^\pm$ production at hadron colliders*, Phys. Rev. D **90** (2014) no.9, 094009 [[arXiv:1409.1460](#) [[hep-ph](#)]].
- [32] A. Broggio, A. Ferroglia, G. Ossola and B. D. Pecjak, *Associated production of a top pair and a W boson at next-to-next-to-leading logarithmic accuracy*, JHEP **1609** (2016) 089 [[arXiv:1607.05303](#) [[hep-ph](#)]].
- [33] A. Kulesza, L. Motyka, D. Schwartländer, T. Stebel and V. Theeuwes, *Associated production of a top quark pair with a heavy electroweak gauge boson at NLO+NNLL accuracy*, Eur. Phys. J. C **79** (2019) no.3, 249 [[arXiv:1812.08622](#) [[hep-ph](#)]].
- [34] R. Frederix and I. Tsinikos, *Subleading EW corrections and spin-correlation effects in $t\bar{t}W$ multi-lepton signatures*, [[arXiv:2004.09552](#) [[hep-ph](#)]].
- [35] P. Artoisenet, R. Frederix, O. Mattelaer and R. Rietkerk, *Automatic spin-entangled decays of heavy resonances in Monte Carlo simulations*, JHEP **03** (2013), 015 [[arXiv:1212.3460](#) [[hep-ph](#)]].
- [36] A. Denner, S. Dittmaier, M. Roth and D. Wackerth, *Predictions for all processes $e^+e^- \rightarrow 4$ fermions + γ* , Nucl. Phys. B **560** (1999) 33 [[hep-ph/9904472](#)].
- [37] A. Denner, S. Dittmaier, M. Roth and L. H. Wieders, *Electroweak corrections to charged-current $e^+e^- \rightarrow 4$ fermion processes: Technical details and further results*, Nucl. Phys. B **724** (2005) 247 Erratum: [Nucl. Phys. B **854** (2012) 504] [[hep-ph/0505042](#)].
- [38] G. Bevilacqua, M. Czakon, A. van Hameren, C. G. Papadopoulos and M. Worek, *Complete off-shell effects in top quark pair hadroproduction with leptonic decay at next-to-leading order*, JHEP **1102** (2011) 083 [[arXiv:1012.4230](#) [[hep-ph](#)]].
- [39] A. Denner, S. Dittmaier, S. Kallweit and S. Pozzorini, *NLO QCD corrections to off-shell top-antitop production with leptonic decays at hadron colliders*, JHEP **1210** (2012) 110 [[arXiv:1207.5018](#) [[hep-ph](#)]].
- [40] N. Kauer and D. Zeppenfeld, *Finite width effects in top quark production at hadron colliders*, Phys. Rev. D **65** (2002), 014021 [[arXiv:hep-ph/0107181](#) [[hep-ph](#)]].
- [41] G. Bevilacqua, M. Czakon, M. V. Garzelli, A. van Hameren, A. Kardos, C. G. Papadopoulos, R. Pittau and M. Worek, *HELAC-NLO*, Comput. Phys. Commun. **184** (2013) 986 [[arXiv:1110.1499](#) [[hep-ph](#)]].
- [42] A. Cafarella, C. G. Papadopoulos and M. Worek, *Helac-Phegas: A Generator for all parton level processes*, Comput. Phys. Commun. **180** (2009) 1941 [[arXiv:0710.2427](#) [[hep-ph](#)]].
- [43] A. van Hameren, *PARNI for importance sampling and density estimation*, Acta Phys. Polon. B **40** (2009) 259 [[arXiv:0710.2448](#) [[hep-ph](#)]].
- [44] A. van Hameren, *Kaleu: A General-Purpose Parton-Level Phase Space Generator*, [[arXiv:1003.4953](#) [[hep-ph](#)]].
- [45] P. Nogueira, *Automatic Feynman graph generation*, J. Comput. Phys. **105** (1993) 279.
- [46] A. van Hameren, C. G. Papadopoulos and R. Pittau, *Automated one-loop calculations: A Proof of concept*, JHEP **0909** (2009) 106 [[arXiv:0903.4665](#) [[hep-ph](#)]].

- [47] G. Ossola, C. G. Papadopoulos and R. Pittau, *Reducing full one-loop amplitudes to scalar integrals at the integrand level*, Nucl. Phys. B **763** (2007) 147 [[hep-ph/0609007](#)].
- [48] G. Ossola, C. G. Papadopoulos and R. Pittau, *CutTools: A Program implementing the OPP reduction method to compute one-loop amplitudes*, JHEP **0803** (2008) 042 [[arXiv:0711.3596](#) [[hep-ph](#)]].
- [49] A. van Hameren, *OneLoop: For the evaluation of one-loop scalar functions*, Comput. Phys. Commun. **182** (2011) 2427 [[arXiv:1007.4716](#) [[hep-ph](#)]].
- [50] M. Czakon, C. G. Papadopoulos and M. Worek, *Polarizing the Dipoles*, JHEP **0908** (2009) 085 [[arXiv:0905.0883](#) [[hep-ph](#)]].
- [51] S. Catani and M. H. Seymour, *A General algorithm for calculating jet cross-sections in NLO QCD*, Nucl. Phys. B **485** (1997) 291 Erratum: [Nucl. Phys. B **510** (1998) 503] [[hep-ph/9605323](#)].
- [52] S. Catani, S. Dittmaier, M. H. Seymour and Z. Trocsanyi, *The Dipole formalism for next-to-leading order QCD calculations with massive partons*, Nucl. Phys. B **627** (2002) 189 [[hep-ph/0201036](#)].
- [53] G. Bevilacqua, M. Czakon, M. Kubocz and M. Worek, *Complete Nagy-Soper subtraction for next-to-leading order calculations in QCD*, JHEP **1310** (2013) 204 [[arXiv:1308.5605](#) [[hep-ph](#)]].
- [54] G. Bevilacqua, M. Czakon, C. G. Papadopoulos, R. Pittau and M. Worek, *Assault on the NLO Wishlist: $pp \rightarrow t\bar{t}b\bar{b}$* , JHEP **0909** (2009) 109 [[arXiv:0907.4723](#) [[hep-ph](#)]].
- [55] M. Czakon, H. B. Hartanto, M. Kraus and M. Worek, *Matching the Nagy-Soper parton shower at next-to-leading order*, JHEP **1506** (2015) 033 [[arXiv:1502.00925](#) [[hep-ph](#)]].
- [56] G. Bevilacqua, H. B. Hartanto, M. Kraus and M. Worek, *Top Quark Pair Production in Association with a Jet with Next-to-Leading-Order QCD Off-Shell Effects at the Large Hadron Collider*, Phys. Rev. Lett. **116** (2016) no.5, 052003 [[arXiv:1509.09242](#) [[hep-ph](#)]].
- [57] G. Bevilacqua, H. B. Hartanto, M. Kraus and M. Worek, *Off-shell Top Quarks with One Jet at the LHC: A comprehensive analysis at NLO QCD*, JHEP **1611** (2016) 098 [[arXiv:1609.01659](#) [[hep-ph](#)]].
- [58] G. Bevilacqua, H. B. Hartanto, M. Kraus, T. Weber and M. Worek, *Hard Photons in Hadroproduction of Top Quarks with Realistic Final States*, JHEP **1810** (2018) 158 [[arXiv:1803.09916](#) [[hep-ph](#)]].
- [59] G. Bevilacqua, H. B. Hartanto, M. Kraus, T. Weber and M. Worek, *Towards constraining Dark Matter at the LHC: Higher order QCD predictions for $t\bar{t} + Z(Z \rightarrow \nu_\ell \bar{\nu}_\ell)$* , JHEP **1911** (2019) 001 [[arXiv:1907.09359](#) [[hep-ph](#)]].
- [60] J. Alwall *et al.*, *A Standard format for Les Houches event files*, Comput. Phys. Commun. **176** (2007) 300 [[hep-ph/0609017](#)].
- [61] I. Antcheva *et al.*, *ROOT: A C++ framework for petabyte data storage, statistical analysis and visualisation*, Comput. Phys. Commun. **180** (2009) 2499 [[arXiv:1508.07749](#) [[physics.data-an](#)]].
- [62] Z. Bern, L. J. Dixon, F. Febres Cordero, S. Höche, H. Ita, D. A. Kosower and D. Maitre, *Ntuples for NLO Events at Hadron Colliders*, Comput. Phys. Commun. **185** (2014) 1443 [[arXiv:1310.7439](#) [[hep-ph](#)]].

- [63] G. Bevilacqua, 2019 (unpublished).
- [64] [ATLAS], *Measurement of the tau lepton reconstruction and identification performance in the ATLAS experiment using pp collisions at $\sqrt{s} = 13$ TeV*, [ATLAS-CONF-2017-029](#).
- [65] V. Khachatryan *et al.* [CMS Collaboration], *Reconstruction and identification of τ lepton decays to hadrons and ν_τ at CMS*, JINST **11** (2016) no.01, P01019 [[arXiv:1510.07488](#) [[physics.ins-det](#)]].
- [66] J. Campbell and T. Neumann, *Precision Phenomenology with MCFM*, JHEP **1912** (2019) 034 [[arXiv:1909.09117](#) [[hep-ph](#)]].
- [67] J. Butterworth *et al.*, *PDF4LHC recommendations for LHC Run II*, J. Phys. G **43** (2016) 023001 [[arXiv:1510.03865](#) [[hep-ph](#)]].
- [68] S. Dulat *et al.*, *New parton distribution functions from a global analysis of quantum chromodynamics*, Phys. Rev. D **93** (2016) no.3, 033006 [[arXiv:1506.07443](#) [[hep-ph](#)]].
- [69] L. A. Harland-Lang, A. D. Martin, P. Motylinski and R. S. Thorne, *Parton distributions in the LHC era: MMHT 2014 PDFs*, Eur. Phys. J. C **75** (2015) no.5, 204 [[arXiv:1412.3989](#) [[hep-ph](#)]].
- [70] R. D. Ball *et al.* [NNPDF Collaboration], *Parton distributions for the LHC Run II*, JHEP **1504** (2015) 040 [[arXiv:1410.8849](#) [[hep-ph](#)]].
- [71] A. Buckley, J. Ferrando, S. Lloyd, K. Nordström, B. Page, M. Rüfenacht, M. Schönherr and G. Watt, *LHAPDF6: parton density access in the LHC precision era*, Eur. Phys. J. C **75** (2015) 132 [[arXiv:1412.7420](#) [[hep-ph](#)]].
- [72] M. Jezabek and J. H. Kühn, *QCD Corrections to Semileptonic Decays of Heavy Quarks*, Nucl. Phys. B **314** (1989) 1.
- [73] K. G. Chetyrkin, R. Harlander, T. Seidensticker and M. Steinhauser, *Second order QCD corrections to $\Gamma(t \rightarrow Wb)$* , Phys. Rev. D **60** (1999) 114015 [[hep-ph/9906273](#)].
- [74] W. Beenakker, S. Dittmaier, M. Krämer, B. Plumper, M. Spira and P. M. Zerwas, *Higgs radiation off top quarks at the Tevatron and the LHC*, Phys. Rev. Lett. **87** (2001) 201805 [[hep-ph/0107081](#)].
- [75] W. Beenakker, S. Dittmaier, M. Krämer, B. Plumper, M. Spira and P. M. Zerwas, *NLO QCD corrections to t anti- t H production in hadron collisions*, Nucl. Phys. B **653** (2003) 151 [[hep-ph/0211352](#)].
- [76] S. Dawson, L. H. Orr, L. Reina and D. Wackerth, *Associated top quark Higgs boson production at the LHC*, Phys. Rev. D **67** (2003) 071503 [[hep-ph/0211438](#)].
- [77] S. Dawson, C. Jackson, L. H. Orr, L. Reina and D. Wackerth, *Associated Higgs production with top quarks at the large hadron collider: NLO QCD corrections*, Phys. Rev. D **68** (2003) 034022 [[hep-ph/0305087](#)].
- [78] A. Lazopoulos, T. McElmurry, K. Melnikov and F. Petriello, *Next-to-leading order QCD corrections to $t\bar{t}Z$ production at the LHC*, Phys. Lett. B **666** (2008) 62 [[arXiv:0804.2220](#) [[hep-ph](#)]].
- [79] A. Kardos, Z. Trocsanyi and C. Papadopoulos, *Top quark pair production in association with a Z-boson at NLO accuracy*, Phys. Rev. D **85** (2012) 054015 [[arXiv:1111.0610](#) [[hep-ph](#)]].
- [80] M. Cacciari, G. P. Salam and G. Soyez, *The anti- k_T jet clustering algorithm* JHEP **0804** (2008) 063, [[arXiv:0802.1189](#) [[hep-ph](#)]].

- [81] G. Aad *et al.* [ATLAS Collaboration], *Muon reconstruction performance of the ATLAS detector in proton-proton collision data at $\sqrt{s} = 13$ TeV*, Eur. Phys. J. C **76** (2016) no.5, 292 [[arXiv:1603.05598](#) [[hep-ex](#)]].
- [82] M. Aaboud *et al.* [ATLAS Collaboration], *Electron reconstruction and identification in the ATLAS experiment using the 2015 and 2016 LHC proton-proton collision data at $\sqrt{s} = 13$ TeV*, Eur. Phys. J. C **79** (2019) no.8, 639 [[arXiv:1902.04655](#) [[physics.ins-det](#)]].
- [83] M. Czakon, D. Heymes and A. Mitov, *Dynamical scales for multi-TeV top-pair production at the LHC*, JHEP **04** (2017), 071 [[arXiv:1606.03350](#) [[hep-ph](#)]].
- [84] G. Bevilacqua, H. Hartanto, M. Kraus, T. Weber and M. Worek, *Off-shell vs on-shell modelling of top quarks in photon associated production*, JHEP **03** (2020), 154 [[arXiv:1912.09999](#) [[hep-ph](#)]].
- [85] V. S. Fadin, V. A. Khoze and A. D. Martin, *How suppressed are the radiative interference effects in heavy instable particle production?*, Phys. Lett. B **320** (1994), 141-144 [[arXiv:hep-ph/9309234](#) [[hep-ph](#)]].